

**MASTER**

**Development of a fuel injection equipment characterisation setup**

Goertz, Noud C.P.

*Award date:*  
2022

[Link to publication](#)

**Disclaimer**

This document contains a student thesis (bachelor's or master's), as authored by a student at Eindhoven University of Technology. Student theses are made available in the TU/e repository upon obtaining the required degree. The grade received is not published on the document as presented in the repository. The required complexity or quality of research of student theses may vary by program, and the required minimum study period may vary in duration.

**General rights**

Copyright and moral rights for the publications made accessible in the public portal are retained by the authors and/or other copyright owners and it is a condition of accessing publications that users recognise and abide by the legal requirements associated with these rights.

- Users may download and print one copy of any publication from the public portal for the purpose of private study or research.
- You may not further distribute the material or use it for any profit-making activity or commercial gain



## Verklaring inzake TU/e Gedragscode Wetenschapsbeoefening in het kader van de Masterscriptie

Ik heb kennis genomen van de TU/e Gedragscode Wetenschapsbeoefening<sup>1</sup>.

Hierbij verklaar ik dat mijn Masterscriptie conform de regels van de TU/e Gedragscode Wetenschapsbeoefening tot stand is gekomen.

Datum

13-6-2022

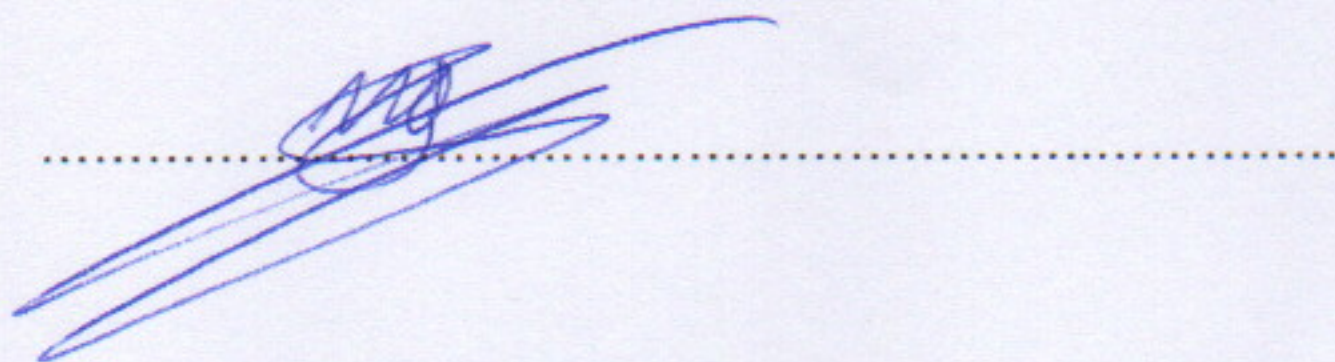
Naam

N.C.P. Goertz

Identiteitsnummer

1000130

Handtekening



Lever de ondertekende verklaring in bij uw facultaire studentenadministratie

<sup>1</sup> Zie: <https://www.tue.nl/universiteit/over-de-universiteit/integriteit/wetenschappelijke-integriteit/>

Hier is ook de Nederlandse Gedragscode Wetenschappelijke Integriteit onderschreven door 6 koepelorganisaties, waaronder de VSNU te vinden. Meer informatie over wetenschappelijke integriteit is te vinden op de websites van de TU/e en de VSNU.



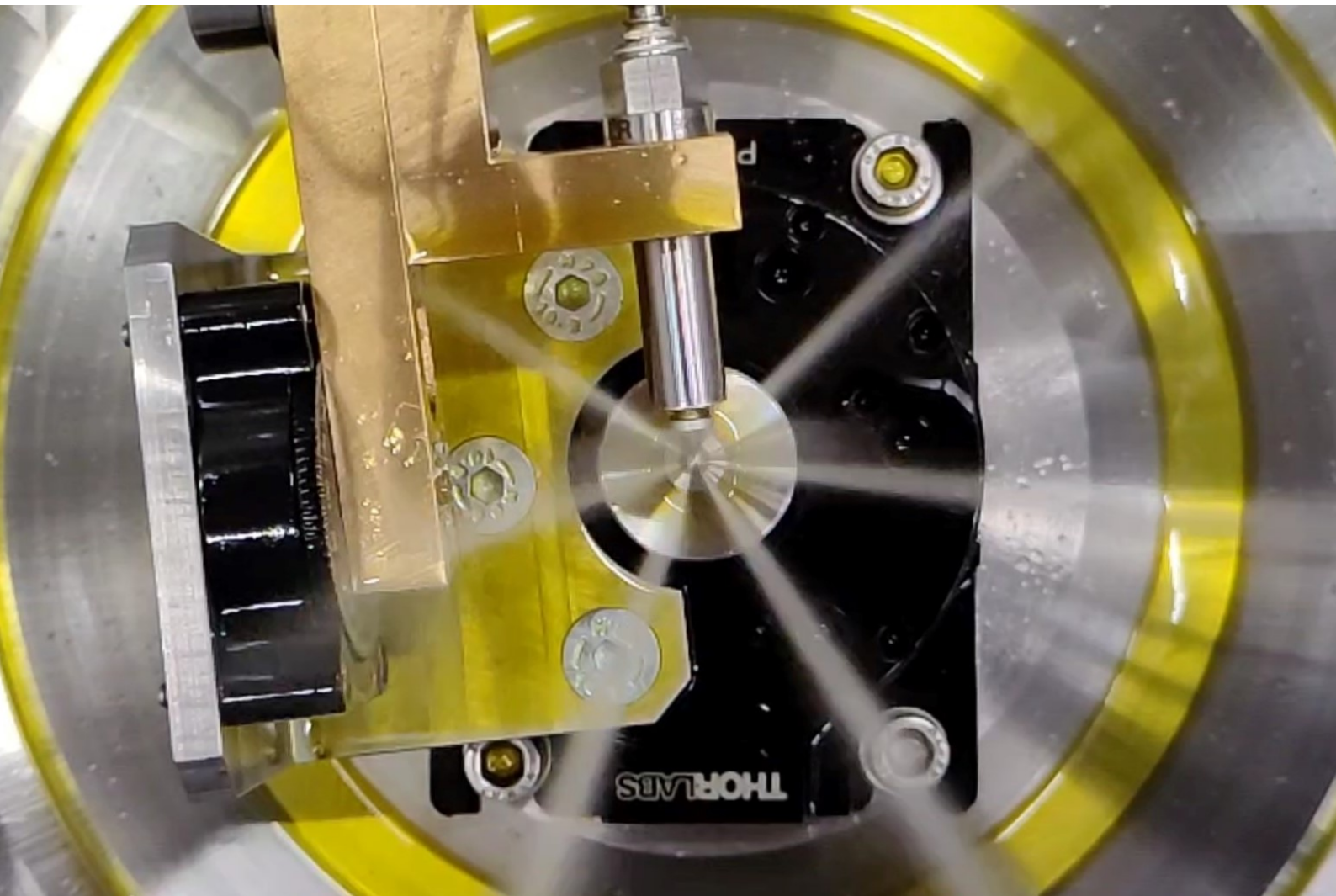
---

Development of a fuel injection equipment  
characterisation setup

---

GRADUATION PROJECT REPORT

N.C.P. (Noud) Goertz



Supervisors:

Dr. Ir. Noud C.J. Maes

Dr. Ir. Xander L.J. Seykens

MSc. Yu Wang

Department of Mechanical Engineering, Power & Flow

June, 2022

# Abstract

In order to limit the burden that global warming is currently already putting on societies, nearly all countries worldwide have committed to the Paris Agreement [1]. One of the aims of the agreement is the limitation of greenhouse gas emissions in transport vehicles, which can be achieved by introducing new fuels and combustion concepts. These fuels can have substantially different properties and characteristics from traditional fuels, such as diesel. Because of these different properties, the behaviour of both the fuel injector and injected fuel spray can change, resulting in completely different combustion behaviour. In order to gain a better understanding of these differences in injection behaviour, an experimental setup must be adopted that can be used for the characterisation of the different fuel and injector types. Unfortunately, such an experimental characterisation setup is currently not present at the Power & Flow research group at the Eindhoven Technical University. Therefore, a new setup is developed for this purpose. In the future, it should accommodate the characterisation of both different injector and different fuel types.

With the use of an extensive literature study, a framework is laid out for the determination of the flow characterisation coefficients for both incompressible liquid, and compressible gaseous nozzle flow. Additionally, previous research regarding injector nozzle characterisation is adopted to select the most suitable measurement method for the experimental setup, which is determined to be the jet impingement force measuring method. This method accommodates direct measurement of the momentum flow rate and, via a secondary experiment, the mass flow rate of the fuel spray. Both parameters are necessary for proper characterisation of the flow characteristics of the injector. Subsequently, an overarching overview of the required components for the physical setup is introduced.

From a set of exploratory experiments on the newly built setup, a number of interesting conclusions can be drawn. The syringe pump has excellent properties regarding the delivery of a stable fuel pressure at start of energising of the injector (SOE), resulting in very minor injection-to-injection differences. Furthermore, the possibility to characterise differences in flow behaviour between individual holes—a distinct advantage of the jet impingement method—is demonstrated, as well as the error sensitivity of the measured signal to a misalignment of the momentum sensor. The influence of the spray target diameter and target-to-nozzle distance on the properties of the measured signal was also investigated.

On the other hand, there are still several aspects of the setup that require further (future) attention. An important point is the unwanted vibration that was observed in all obtained measurement data, that is hypothesised to originate from the injector needle actuation. In addition, the exact effects of the syringe pump's pressure feedback on the rail pressure during the injection phase are not yet well understood.

# Contents

<b>1</b>	<b>Introduction</b>	<b>5</b>
1.1	Research questions . . . . .	6
1.2	Report structure . . . . .	6
<b>2</b>	<b>Background and theory</b>	<b>8</b>
2.1	Injection strategies for direct injection ICE . . . . .	8
2.2	Common rail fuel injection equipment . . . . .	10
2.3	Injector characterisation . . . . .	11
2.3.1	Liquid nozzle flow characterisation . . . . .	11
2.3.2	Gaseous nozzle flow characterisation . . . . .	13
<b>3</b>	<b>Measuring method selection</b>	<b>16</b>
3.1	Setup requirements, preferences, and constraints . . . . .	16
3.1.1	Requirements . . . . .	16
3.1.2	Preferences . . . . .	16
3.1.3	Constraints . . . . .	17
3.2	Measurement methods . . . . .	17
3.2.1	Bosch rate of injection method . . . . .	17
3.2.2	Zeuch rate of injection method . . . . .	19
3.2.3	Jet impingement force method . . . . .	20
3.2.4	Commercial solutions . . . . .	21
3.3	Method selection . . . . .	22
<b>4</b>	<b>Experimental setup design</b>	<b>24</b>
4.1	System overview . . . . .	24
4.2	Fuel delivery system . . . . .	25
4.2.1	Fuel storage and filtration . . . . .	25
4.2.2	High-pressure pump . . . . .	26
4.2.3	Fuel lines . . . . .	28
4.3	Injection chamber . . . . .	29
4.3.1	Injector mounting . . . . .	29
4.3.2	Sensor alignment . . . . .	30
4.4	Sensors . . . . .	32
4.4.1	Rail pressure sensor . . . . .	32
4.4.2	Momentum sensor . . . . .	32
4.4.3	Spray target material and geometry . . . . .	36
4.5	Momentum- to mass flow rate correlation . . . . .	37
4.6	Data acquisition and injector actuation . . . . .	39
4.7	Implementation of gaseous hydrogen injections . . . . .	41
<b>5</b>	<b>Setup functionality verification and first measurements</b>	<b>42</b>
5.1	Injector solenoid actuation . . . . .	43
5.2	Injection-to-injection variation . . . . .	44
5.3	Injector needle vibration . . . . .	45
5.4	Sensor alignment sensitivity . . . . .	46
5.5	Target size and target-to-nozzle distance . . . . .	47
5.6	Hole-to-hole variation . . . . .	48

<b>6</b>	<b>Conclusions</b>	<b>50</b>
<b>7</b>	<b>Recommendations for future work</b>	<b>52</b>
	<b>References</b>	<b>54</b>
<b>A</b>	<b>Pressure sensor calibration</b>	<b>57</b>

# List of Tables

1	Properties and measurement capabilities for main measurement methods . . . . .	23
2	Kistler 9215A and 9217A technical specifications [2] . . . . .	35
3	Baseline injection parameters . . . . .	43

# List of Figures

2.1	Phases of combustion in an internal combustion engine [3] . . . . .	9
2.2	Visualisation of multiple injection events [4] . . . . .	10
2.3	Schematic of diesel common rail FIE . . . . .	11
2.4	Schematic diagram of underexpanded jet near nozzle exit [5] . . . . .	14
2.5	Comparison between different gaseous injection penetration models . . . . .	15
3.1	Schematic of Bosch ROI device [6] . . . . .	18
3.2	Schematic of Zeuch ROI device [6] . . . . .	19
3.3	Schematic of jet impingement force method [7] . . . . .	21
4.1	Schematic of the experimental setup designed for liquid fuels . . . . .	25
4.2	Schematic of syringe pump working principle . . . . .	28
4.3	Overview of physical setup and injection chamber . . . . .	29
4.4	Exploded view of injector chamber base plate and injector clamp-down components . . . . .	30
4.5	Schematic representation of the rotation and translation axes of the momentum sensor . . . . .	31
4.6	Schematic representation showing concentricity between the injector nozzles and alignment axes . . . . .	31
4.7	Differences in component layouts between PE force and pressure sensors. <i>Derived from</i> [8] . . . . .	34
4.8	Geometry of selected spray targets with different face diameters. Depicted diameters in millimetres . . . . .	37
4.9	Labview™ front panel of developed DAQ VI . . . . .	40
4.10	Schematic visualising the dataflow in the developed Labview™ DAQ VI . . . . .	40
5.1	Effects of too high injection frequency on rail pressure. Targeted pressure of 340 bar, injection frequency of 20 Hz . . . . .	42
5.2	TTL actuation voltage and injector current . . . . .	43
5.3	Momentum flow rate of 5 individual injections in a recording. All cases with ET of 1 ms, target diameter of 7.5 mm, and a target-to-nozzle distance of 7.5 mm . . . . .	44
5.4	Rail pressure traces belonging to injections of Figure 5.3 . . . . .	45
5.5	Suspected influence of needle actuation vibration on force measurement. All cases with ET of 1 ms, target diameter of 7.5 mm, and a target-to-nozzle distance of 7.5 mm . . . . .	46
5.6	Influence of sensor misalignment on recorded momentum flow rate signal. All cases with ET of 1 ms, target diameter of 7.5 mm, and a target-to-nozzle distance of 7.5 mm . . . . .	46
5.7	Influence of spray target diameter (D) on measured momentum flow rate. All cases with 1 ms ET, and 7.5 mm target-to-nozzle distance . . . . .	47
5.8	Influence of target-to-nozzle distance (L) on measured momentum flow rate. All cases with 1 ms ET, and 10 mm target diameter . . . . .	48

5.9	Variation in momentum flow rate between holes in the fuel injector. All cases with ET of 1 ms, target diameter of 7.5 mm, and a target-to-nozzle distance of 7.5 mm . . . . .	48
A.1	Replication of a static force calibration for piezoelectric sensors. . . . .	57



# 1 Introduction

The times in which we are currently living can be effectively epitomised as the *era of energy transition*. The move from fossil energy sources to renewable sources is included in the Paris Climate Agreement, and aims to limit the global warming temperature effects caused by i.a. CO<sub>2</sub> and other greenhouse gases. [1]. A substantial portion of this carbon pollution can be traced back to the transportation sector [9], which still relies heavily on fossil sources—to be more precise, fossil fuels—as its main energy carrier. In an attempt to lower these greenhouse gas (GHG) emissions of transport vehicles, stringent regulations focusing on restricting pollutant and internal combustion engine (ICE) emissions have been introduced. This becomes more difficult as the product is optimised; the emissions of GHG is an inherent concept attached to ICE, as long as fossil hydrocarbons are used as fuel.

An interesting prospect is the use of hydrogen as energy carrier: because its inherent molecular structure contains no carbon atoms it is suitable as a possible means of targeting zero-carbon emission replacement for fossil fuels. When used as a replacement in hydrogen internal combustion engines (HICE), however, small amounts of NO<sub>x</sub> can nevertheless be emitted. Therefore, it can still be inferior to the zero-tailpipe emissions that are characteristic of EV and hydrogen fuel cell electric vehicles (HFCEV) [10].

For ICE, whether fossil or hydrogen powered, the fuel injection equipment (FIE) ensures that the correct amount of fuel is delivered to the cylinder at the correct time, such that the engine can run at the highest efficiency with lowest emissions. With recent trends moving towards more advanced combustion concepts, more flexible fuel injections are required: under ideal conditions contemporary engines often use (multiple) pilot, main, and post injections within a very short time span to improve emissions, combustion noise, and fuel economy. Simultaneously, a wide variety of new (research) fuels are developed for use in future combustion engines. Logically, these fuels have different properties and characteristics. As a result, both the injection behaviour and optimised injector design differs for every fuel type. To gain a better understanding of the differences in injection behaviour between fuel types and other injection parameters, it is absolutely vital to establish an experimental setup that can aid in this typification.

Currently, within the Power & Flow research group at the Eindhoven Technical University, no such injector characterisation setup is available. Therefore, the research group has to rely on manufacturer or literature data when wanting to compare injector behaviour. Typically, this data is not very accurate and does not provide the researchers with the exact information they need. Additionally, the available data often does not cover prototype hardware, a necessity in an academic laboratory at the forefront of research. For this reason, there is a need for a FIE characterisation setup at TU/e, that will allow the researchers to conduct specific measurements on injector and injections. The setup will provide data that is crucial for numerical and experimental combustion research, and will enable quantification of injector dynamics that is important for engine control and diagnostics. The measurement capabilities of the setup will specifically focus on the mass- and momentum flow rate of the fuel, two parameters that are especially important for describing the fuel spray characteristics in an injection.

## 1.1 Research questions

The research questions that apply to this graduation project are as follows:

- “Which measurement technique is the best suitable for the determination of mass- and momentum flow rate, and injector characterisation coefficients?” Every proposed measurement method inherits certain (dis)advantages; since available time is limited the most promising measurement technique must be selected. This choice must be carefully made, taking performance, flexibility in measuring capabilities and ease of development and use into account.
- “Can a single measurement technique setup suffice in adequately determining both the mass flow rate  $\dot{m}$  and momentum flow rate  $\dot{M}$ ? Can the desired parameters be directly determined from the experimental data?” Although certain techniques enable measurement of both parameters, adequate accuracy and precision must be verified when using a single measurement technique setup. Is there a need for assumptions in calculating the desired quantities, that might influence the acquired results? Are there other factors which might influence the level of accuracy of the experiments?
- “How does the phase of the fuel influence the flow behaviour, and what effect does this have on the robustness of the measurements?” Since the setup should ideally be able to characterise both gaseous and liquid fuel injectors, it is important to investigate the different properties and their effects on the measurements. It might be necessary to separately develop complete sub-components and measuring methods for the respective injector types.
- “What components are needed for the experimental setup? How does the choice for a particular component type influence the performance of the setup?” Certain options arise for the realisation of the components of the setup, each with their (dis)advantages. The most appropriate options must be investigated and realised.
- “After initial testing, can aspects of the setup design be identified that do not function as expected? How can these aspects be improved upon?” As with the majority of prototypes, there will be aspects of the setup that, initially, do not completely function as intended. Can the setup be made more user-friendly? Simplifying the measurement setup where possible increases reliability and decreases costs.

## 1.2 Report structure

In section 2, the relevant theory for this project is introduced. Background information about diesel and hydrogen engines is presented, and a typical injection profile with the associated injection phases is introduced. Additionally, the approach for the calculation of both liquid and gaseous injector nozzle coefficients is presented.

In section 3, the relevant measurement techniques for acquiring the FIE characterisation measurement data are introduced. Later in the section, the most promising measurement technique is selected using a framework of requirements, preferences, constraints and measuring properties that the setup ought to adhere to.

Section 4 focuses on the identification of the components that are necessary for the chosen measurement concept to evolve into a physical, fully-functioning experimental setup.



Later in the section, these system components are addressed in more detail, including the fuel delivery system, choice of high-pressure pump type, injection chamber design, and choice of main sensing transducer type. Furthermore, the framework for determining both the mass- and momentum flow rate using a single measuring device is laid out. Finally, the most important features of the data acquisition system are discussed.

In section 5, the results of the initial experiments using the developed measurement setup are presented. Insight is given into the specific behaviour of the current setup during measurements. Injection-to-injection, hole-to-hole, injection-averaged, and sensor alignment sensitivity is discussed.

Finally, in section 6, the reader is presented with the main conclusions of the project. A list of suggested improvements on the physical setup, as well as future points of consideration concerning the quality of the measurement data, is handed to the reader.

## 2 Background and theory

Whilst diesel powered engines almost exclusively make use of direct injection, hydrogen combustion engines that have been developed can generally be placed in two categories; port fuel injection (PFI) and direct injection (DI), where the fuel is mostly ignited through spark ignition (SI). PFI ICE inject the hydrogen into the intake runner, upstream of the intake valve. The advantage of this system is that it can be installed relatively easy on already existing gasoline engines with similar technology. The chemical properties of hydrogen, however, limit the effectiveness of this solution. Although it has the highest auto-ignition temperature and RON of all common fuels (therefore suggesting high resistance to knocking), its minimum ignition energy in air at stoichiometry is approximately one order of magnitude smaller than that of other hydrocarbon fuels [11]. This indicates that hot spots in the combustion chamber can quite easily ignite the hydrogen fuel, therefore leading to unintended pre-ignition resulting in unwanted engine knock. This is especially applicable to PFI ICE because—contrary to DI ICE—the fuel is injected and mixing much earlier than ignition is required. A second inconvenience is the relatively small quenching distance when compared to other fuels. The quenching distance typifies the smallest distance between two parallel surfaces that allows the propagation of a flame. The small quenching distance of hydrogen can result in higher heat transfer losses, since steeper temperature gradients are expected near the combustion chamber walls. In PFI engines, the small quenching distance together with the high flame speed of hydrogen can lead to harmful backfiring into the intake manifold [12].

Since in DI ICE hydrogen is injected only after the intake valve is closed, backfiring into the intake can be completely avoided [13]. Additionally, pre-ignition of hydrogen can be avoided by limiting the exposure time of hydrogen to the hot spots in the combustion chamber. Because the fuel is injected directly into the combustion chamber, the injector design, however, must allow for a high enough injection pressure in order to overcome the maximum in-cylinder pressure. The importance of injector design is furthermore seen in the findings that the injection umbrella angle strongly impacts the engine performance by minimising wall heat loss if the hydrogen jets are spaced appropriately [14]. The implementation of multiple injection events, as in common rail diesel DI ICE, can result in large reductions of  $\text{NO}_x$  emissions at different engine loads, whilst maintaining equal engine efficiency compared to a single injection event [15]. Whether diesel, hydrogen or any other fuel is used, characterising the dynamic behaviour of injectors is important for the understanding of injected quantity, the mixing process, and the simulation of these parameters.

### 2.1 Injection strategies for direct injection ICE

In diesel engines, torque at the crankshaft is controlled by varying the duration and flow rate of the fuel injection event. In the conventional case, only a single injection event takes place during each engine cycle. During the compression stroke near TDC at the start of injection (SOI, Figure 2.1), the fuel spray mixes with hot pressurised air. It atomises and vaporises, after which combustion starts. During this so-called ignition delay (Figure 2.1), a portion of the injected fuel undergoes initial low-temperature chemistry reactions and, subsequently, burns rapidly once high-temperature ignition commences. This is referred to as the “premixed peak”, where sudden and high heat release rates are observed as seen in Figure 2.1; this “premixed peak” is what is associated with the characteristic



diesel engine combustion noise. Generally, the combustion noise increases with increasing pressure rise from the premixed peak. Next, the bulk of the injected fuel is combusted during the rate-controlled combustion phase. The rate of heat release is lower and the rate of combustion is governed by the injection rate and mixing rate of the fuel and air. During the combustion phase  $\text{NO}_x$  is formed in areas where the temperature is sufficiently high to oxidise the nitrogen present in air.

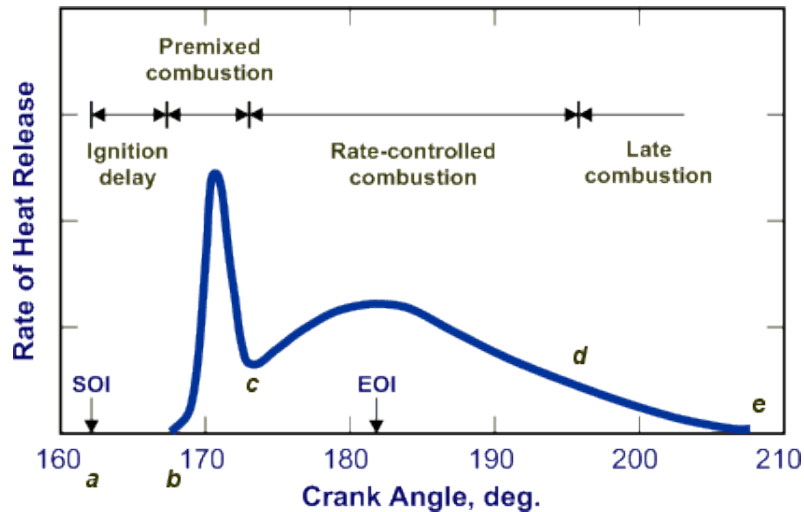


Figure 2.1: Phases of combustion in an internal combustion engine [3]

The quest for improvements in levels of combustion noise,  $\text{NO}_x$ , and PM emissions has led to the introduction of a number of solutions that improve the performance of internal combustion engines. Examples include (variable geometry) turbocharging, charge air cooling, exhaust gas recirculation (EGR) and higher pressure fuel injection systems [16]. At a given injection duration, the higher injection pressure allows for the injection of an equal fuel quantity through a smaller injector nozzle. This is favourable, because the mixing between fuel and air is vastly improved, and which lowers PM emissions [4], albeit at the cost of some  $\text{NO}_x$  emission increase. A second development was the introduction of multiple injection events within one engine cycle, which was largely made possible by developments in common rail FIE. A main injection event accompanied by several smaller ones has allowed the manufacturers to combat the aforementioned problems that arise with diesel combustion. The different injection events, as shown in Figure 2.2, are classified as [17]:

- **Pre-injection.** Also known as pilot injections. A small quantity of fuel injected well before TDC, that gives rise to a more reactive combustion chamber environment and therefore decreases ignition delay of the main injection. In addition, a shorter ignition delay decreases the heat release peak in premixed combustion, which greatly reduces combustion noise.
- **Main injection.** As the name suggests, this injection ensures that the torque requested by the ECU is produced by adjusting the rate and duration of injection, also known as “rate shaping”. These parameters can have a substantial influence on the thermal efficiency of the engine. At high load or RPM, it is important that the injector can inject the requested amount of fuel in the available time window, therefore rate shape optimisation is generally not used in such situations.

- **Close-coupled post-injection.** A relatively short injection, after the main injection but before the end of the combustion process. The purpose of this injection is the reduction of PM emissions. The extra momentum introduced by this post-injection improves mixing and, therefore, increases soot oxidation.
- **Late post-injection.** Similarly sized to the close-coupled post-injection, although occurring much later after the end of the combustion process and, therefore, not necessarily burned in-cylinder. Injections of this kind are typically used to increase the exhaust gas temperature and enthalpy to improve the performance of the engine aftertreatment system (EAS). Further use might be regeneration of  $\text{NO}_x$  adsorbers, which need rich conditions to function effectively.

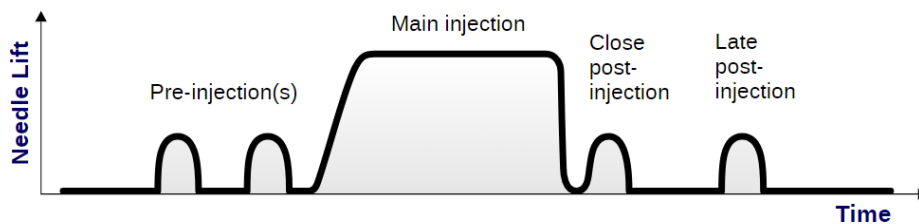


Figure 2.2: Visualisation of multiple injection events [4]

## 2.2 Common rail fuel injection equipment

As shown in Figure 2.3, in common rail fuel injection equipment fuel is pumped up from the fuel tank by a low-pressure lift pump after which it flows through a fuel filter, prior to entering the high-pressure fuel pump. This pump delivers fuel at a constant high-pressure to the common pressure accumulator, referred to as the (common) rail, which is coupled to the injectors. The electronic control unit (ECU) controls the injectors operating parameters and rail fuel pressure, making sure that the correct amount of fuel is delivered to the cylinders at the right time. Other than common rail, there are two widely used FIE systems: pump-line-nozzle (PLN) and unit injector (UI). In PLN systems, the injectors are fed by a central cam-driven unit pump via individual equal-length high-pressure lines. In UI systems, the unit incorporates the high-pressure pump, metering device, and injector into a single unit, thereby eliminating the fuel lines that may suffer from pressure wave interference. The common rail system is however superior to the two other categories in three key areas [18]. The first is the fuel pressure, which in common rail systems is independent of the crankshaft speed and load. This accommodates flexibility in both injection timing and cumulative mass flow of the injector. Secondly, the layout of the high-pressure pump lowers the peak torque demand of the pump on the engine. Thirdly, solenoid injectors incorporated into common rail layouts allow for unprecedented flexibility in rate-shaping capabilities and the implementation of a multitude of injection events, allowing for multiple pre- and post-injections.

For hydrogen DI ICE, existing common rail FIE for diesel DI ICE architecture can be used with only a couple of modifications [19]. The common rail injector design characteristics are based on the use of diesel as both the (lubricating) fuel and the hydraulic working fluid, as its compressibility is relatively low. For adaptation to hydrogen gas, the injector uses two “supply lines”; one with hydrogen gas to be injected into the combustion



chamber, and one for the diesel working fluid for the hydraulic control of the injector needle. The high compressibility and low lubricative properties of the hydrogen gas provide poor properties as a working fluid for the control and durability of the injector, therefore diesel is preferred as the working fluid.

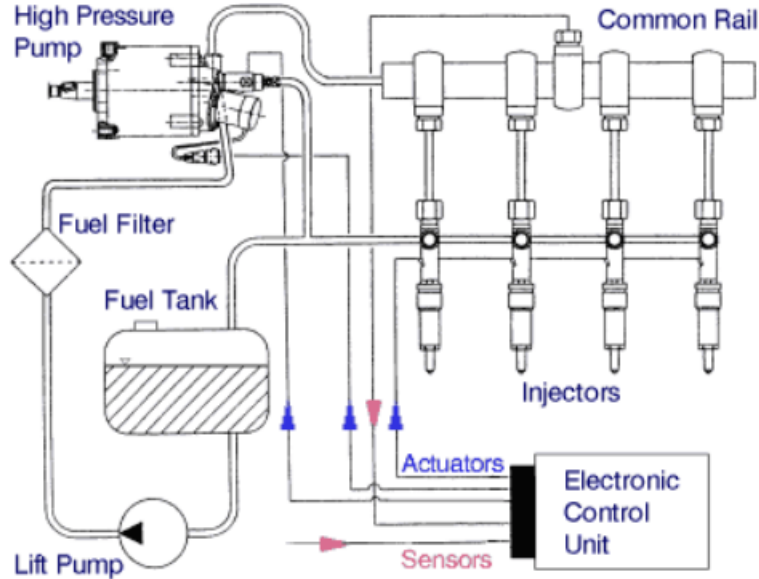


Figure 2.3: Schematic of diesel common rail FIE

## 2.3 Injector characterisation

In combustion engines, the characteristics of the fuel sprays entering the combustion chamber greatly influence the combustion performance. The injector discharge process is generally characterised by two parameters: fuel mass flow rate and momentum flow rate. The former assures supplying the proper amount of fuel at certain operation condition, whilst the latter determines the level of air entrainment which is important for efficient combustion. Both parameters are essential inputs for numerical combustion research. Results from numerical combustion research are often used for the calibration of engine control software, and can support in interpreting measurement data from combustion experiments. The mass and momentum flow rate can be evaluated using Bernoulli's equation. However, their behaviour in practice differ from the theoretical values, and hence, some dimensionless coefficients are employed to characterise these differences.

### 2.3.1 Liquid nozzle flow characterisation

At (ideal) steady-state conditions for a frictionless incompressible flow, Bernoulli's equation gives the following expression for the nozzle velocity:

$$u_0 = \sqrt{\frac{2\Delta p}{\rho_f}}, \quad (1)$$

where  $\Delta p$  [Pa] is the pressure difference between the injection pressure and ambient (in-cylinder) pressure, and  $\rho_f$  [kg/m<sup>3</sup>] the density of the fuel. The theoretical mass flow rate  $\dot{m}_0$  [kg/s] through the nozzle depends on this same velocity:

$$\dot{m}_0 = \rho_f \cdot A_0 \cdot u_0, \quad (2)$$

with  $A_0$  [m<sup>2</sup>] the geometric area of the nozzle orifice perpendicular to the direction of the flow. Similarly, the theoretical momentum flow rate  $\dot{M}_0$  [kg·m/s<sup>2</sup>] follows by

$$\dot{M}_0 = \dot{m}_0 \cdot u_0 = \rho_f \cdot A_0 \cdot u_0^2. \quad (3)$$

Note that  $\dot{m}_0$  and  $\dot{M}_0$  are only theoretical quantities; the actual effective mass- and momentum flow rate from the nozzle usually is substantially different due to geometric influences and flow instabilities. An important example is cavitation, a phenomenon where vapour bubbles appear in the liquid in areas where the local fuel pressure is below the vapour pressure. In injector nozzles this pressure drop can be observed at the nozzle entrance, where the fluid flow undergoes a sudden change in direction from the relatively large injector sac to the nozzle orifice. The vapour cavities effectively decreases the size of nozzle area: this results in an effective area  $A_{eff}$  that can be connected to the theoretical ideal nozzle area  $A_0$  via the area contraction coefficient  $C_a$  [-], which is equal to  $A_{eff}/A_0$  [20]. Additionally, the flow velocity is affected by the vapour cavities that lower wall friction. Hence, the effective injection velocity  $u_{eff}$  [m/s] differs from the ideal velocity. The velocity coefficient  $C_v$  [-] correlates these two parameters to each other, and is equal to  $u_{eff}/u_0$ . The actual mass- and momentum flow rates  $\dot{m}$  and  $\dot{M}$ , respectively, are therefore found through the use of the effective orifice area and velocity,

$$\dot{m} = \rho_f \cdot A_{eff} \cdot u_{eff}, \quad (4)$$

$$\text{and } \dot{M} = \rho_f \cdot A_{eff} \cdot u_{eff}^2. \quad (5)$$

Note that the mass flow rate can be rewritten to a form where it is a function of momentum flow rate:

$$u_{eff} = \sqrt{\frac{\dot{M}}{\rho_f \cdot A_{eff}}} \quad (6)$$

$$\rightarrow \dot{m} = \rho_f \cdot A_{eff} \cdot \sqrt{\frac{\dot{M}}{\rho_f \cdot A_{eff}}} = \sqrt{\rho_f \cdot A_{eff} \cdot \dot{M}} = \sqrt{\rho_f \cdot C_a \cdot A_0 \cdot \dot{M}}. \quad (7)$$

The two other characterisation coefficients that describe the difference between theoretical and actual behaviour are the discharge coefficient  $C_d$  [-] and momentum coefficient  $C_M$  [-]. The discharge coefficient  $C_d$  shows the ratio of actual mass flow rate  $\dot{m}$  over ideal mass flow rate  $\dot{m}_0$ :

$$C_d = \frac{\dot{m}}{\dot{m}_0} = \frac{\sqrt{\rho_f \cdot A_{eff} \cdot \dot{M}}}{\rho_f \cdot A_0 \cdot u_0} = \frac{\sqrt{\rho_f \cdot C_a \cdot A_0 \cdot \dot{M}}}{\rho_f \cdot A_0 \cdot u_0} = \frac{\sqrt{\rho_f \cdot C_a \cdot A_0 \cdot \dot{M}}}{A_0 \sqrt{2\rho_f \Delta p}} \quad (8)$$

$$= \sqrt{\frac{C_a \cdot \dot{M}}{2A_0 \cdot \Delta p}}. \quad (9)$$

Hence, in cases where no cavitation is present,  $C_a$  is equal to 1 and the discharge coefficient can be determined using only the momentum flow rate. Also note that  $C_d$  can be described as the product of  $C_a$  and  $C_v$  when Equation 4 is inserted into Equation 8. Similarly, the momentum coefficient can be described as a function of the other injector coefficients:

$$C_M = \frac{\dot{M}}{\dot{M}_0} = \frac{\rho_f \cdot A_{eff} \cdot u_{eff}^2}{\rho_f \cdot A_0 \cdot u_0^2} = C_a \cdot C_v^2 = C_d \cdot C_v. \quad (10)$$

As seen in the previous derivations, the characterisation coefficients can only be described when the real mass- and momentum flow rate  $\dot{m}$  and  $\dot{M}$  are known. The parameters can be measured from the steady-state portion of a fuel injection.



### 2.3.2 Gaseous nozzle flow characterisation

The equations that are used above to describe the mass- and momentum flow rate are only applicable to ideal, incompressible fluids. For ideal-like, compressible isentropic fluid flow—as is the case with most gases—the formula for theoretical mass flow rate is given by [5]:

$$\dot{m}_0 = \rho_{f,0} \cdot A_0 \cdot u_0 = A_0 \cdot \sqrt{2p_0 \cdot \rho_{f,0} \cdot \frac{\kappa}{\kappa - 1} \cdot \left(\frac{p_1}{p_0}\right)^{2/\kappa} \cdot \left[1 - \left(\frac{p_1}{p_0}\right)^{(\kappa-1)/\kappa}\right]}, \quad (11)$$

where the subscripts 0 and 1 refer respectively to the upstream and downstream conditions of the nozzle, and  $\kappa$  is the specific heat ratio of the gas. In compressible flow theory, if the velocity of the flow reaches the speed of sound in the medium (i.e. Mach 1), changes in pressure can no longer be communicated upstream since the propagation of these pressure changes are limited by the speed of sound. Inside a nozzle, this essentially isolates the upstream from the downstream portion. Therefore, a reduction in downstream pressure will no longer have an effect on the flow rate since the pressure difference is not “communicated” to the upstream portion of the nozzle. The phenomenon is referred to as “choked flow”, and occurs when

$$\frac{p_0}{p_1} > \left(\frac{2}{\kappa + 1}\right)^{-\kappa/(\kappa-1)}. \quad (12)$$

For hydrogen, with  $\kappa=1.41$ , choked flow therefore occurs when the reservoir to ambient pressure ratio is higher than 1.90. The critical—choked—pressure, density, velocity, and temperature at the nozzle exit at these conditions are given by:

$$p^* = p_0 \left(\frac{2}{\kappa + 1}\right)^{\kappa/(\kappa-1)}, \quad (13)$$

$$\rho^* = \rho_0 \left(\frac{p^*}{p_0}\right)^{1/\kappa} = \rho_0 \cdot \left(\frac{2}{\kappa + 1}\right)^{1/(\kappa-1)}, \quad (14)$$

$$u^* = \sqrt{\kappa \frac{p^*}{\rho^*}} = \sqrt{\frac{2\kappa}{\kappa + 1} \frac{p_0}{\rho_0}}, \quad (15)$$

$$T^* = T_0 \left(\frac{2}{\kappa + 1}\right), \quad (16)$$

where the asterix represents the critical condition. Hence, the maximum mass flow rate at the nozzle for choked conditions is obtained by inserting  $\rho^*$  and  $u^*$  into Equation 11:

$$\dot{m}_{0,choked} = \rho^* \cdot A_0 \cdot u^* = \rho_0 \cdot A_0 \left(\kappa \frac{p_0}{\rho_0}\right)^{1/2} \cdot \left(\frac{2}{\kappa + 1}\right)^{(\kappa+1)/2(\kappa-1)}. \quad (17)$$

Indeed, Equation 17 shows that, at choked flow conditions, the maximum mass flow rate does not depend on the pressure difference, but only on the upstream pressure. As the flow velocity is limited by the mach number, the only way to increase mass flow is by increasing the density via the upstream pressure. The same applies to the momentum flow rate which is, analogous to Equation 3, written as

$$\dot{M}_{0,choked} = \rho^* \cdot A_0 \cdot u^{*2} = A_0 \cdot \kappa \cdot p_0 \left(\frac{2}{\kappa + 1}\right)^{\kappa/(\kappa-1)}. \quad (18)$$

Note that both Equation 17 and 18 assume no (viscous) flow losses. Therefore, they indicate the maximum theoretical values. Similar coefficients as described in section 2.3.1 can be introduced to compute actual numbers. They can be obtained following the same approach as described in that section.

In the modelling of the high-pressure gaseous jet as it leaves the nozzle exit, these coefficients are often implemented. Hill and Ouellette [21] developed a jet model that described the tip penetration as a function of time. The model, built on the assumption of conservation of momentum throughout the jet, has been validated for highly underexpanding jets with pressure ratios of up to 70. The model assumes that fuel supply pressure is equal to the fuel pressure at the nozzle exit. Hajialimohammadi et al. have shown that this is a flawed assumption for gaseous fluids. Essentially, they introduce an “effective” pressure that improves the encapsulation of compressible behaviour in the fuel supply reservoir. The effective pressure ratio to the ambient pressure is approximated using the Newton-Raphson method, and acts as a certain loss coefficient since the model now accounts for the pressure loss at the nozzle exit [22].

A model that incorporates an actual discharge coefficient—and thus shows the need for a characterisation tool—was developed by Tsujimura et al. [5]. Their model includes another often-observed phenomenon in highly underexpanded jets: the Mach shock disc. For underexpanded gas flow, the pressure at the nozzle exit is much higher than the ambient pressure, and therefore expansion of the gas takes place outside the nozzle. This indicates that the gas flow is described by a larger source starting from the Mach disc rather than from the actual nozzle, which is referred to as the “pseudo-diameter” [23][24].

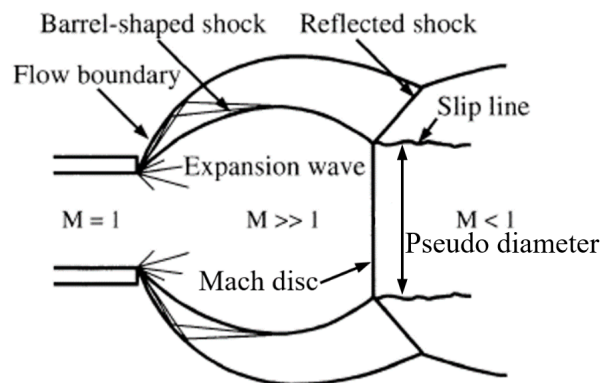


Figure 2.4: Schematic diagram of underexpanded jet near nozzle exit [5]

As Figure 2.4 shows, directly downstream of the nozzle the flow expands and accelerates. As these waves meet the outer flow boundary, and reflect as compression waves, they merge and form a barrel-shaped shock. The supersonic flow inside the barrel-shaped shock is capped by a normal shock referred to as the Mach disc, whose diameter is equal to the pseudo-diameter. It can be assumed that ambient gas cannot be entrained into the barrel-shaped shock, and that the gas pressure at the Mach disc falls to ambient pressure. Therefore, the pseudo-diameter can be calculated via conservation of mass between the nozzle exit and Mach disc according to:

$$d_{MD} = d_0 \left[ C_d \frac{p_0}{p_1} \left( \frac{2}{\kappa + 1} \right)^{(\kappa+1)/2(\kappa-1)} \right]^{1/2}, \quad (19)$$

where  $d_0$  is equal to the nozzle diameter. The length of the barrel-shaped shock can be

calculated by an empirical correlation originally originally introduced by Ewan et al. [24]:

$$L_B = 0.77d_0 + 0.068d_0^{1.35} \frac{p_0}{p_1} \left( \frac{2}{\kappa + 1} \right)^{\kappa/(\kappa-1)}. \quad (20)$$

Tsujimura et al., similar to Hill and Ouellette, developed a jet penetration model based on conservation of momentum in the jet, that includes the discharge coefficient  $C_d$  to represent the losses at the nozzle exit [5]. Contrary to the models by Hill and Ouellette and Hajjalimohammadi et al., the model by Tsujimura et al. explicitly adds the length of the barrel-shaped shock as a parameter in the correlation. The correlation is given by

$$x(t) = a \left[ C_d \cdot \kappa \cdot \frac{p_0}{\rho_1} \left( \frac{2}{\kappa + 1} \right)^{(\kappa+1)/2(\kappa-1)} \right]^{1/4} \cdot \sqrt{d_0 \cdot t / \tan(\theta)} + L_B, \quad (21)$$

where  $a$  is an experimental constant equal to  $1.14 \pm 0.11$ , and  $\theta$  half of the jet dispersion angle. The spray penetration models by Hill and Ouellette, Hajjalimohammadi et al., and Tsujimura et al. are visualised for a certain set of parameters in Figure 2.5. Note the instantaneous penetration length equal to the barrel-shaped shock near  $t = 0$  for the model of Tsujimura et al., and the slower speed of penetration in the model by Hajjalimohammadi et al. following the approximation of the effective pressure near the nozzle exit. The penetration length correlations in the three models are all a function of  $\sqrt{t}$ , marking a power function of the form  $f(t) = at^{0.5}$  where the coefficient  $a$  is formed by the ambient and reservoir parameters. The power function indicates that in space-constrained cylinders, the fuel jet could reach the cylinder wall within several milliseconds, meaning the spray-wall and/or flame-wall impingement could still be a research issue for hydrogen DI engines.

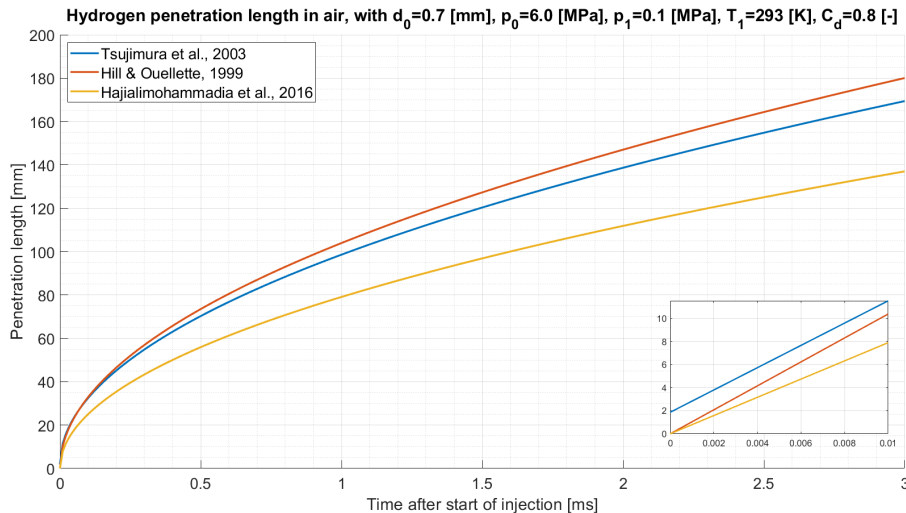


Figure 2.5: Comparison between different gaseous injection penetration models



# 3 Measuring method selection

In this section, the different measuring methods applicable to FIE characterisation are introduced, and based on a set of setup requirements, preferences, and constraints, the most suitable measuring method is selected for further development.

## 3.1 Setup requirements, preferences, and constraints

The features that the experimental setup (preferably) must adhere to can be arranged in three categories, namely requirements, preferences, and constraints (RPC's). Requirements refer to features and functions that are explicitly needed by the researcher to guarantee sufficient performance and testing flexibility. Preferences are not necessary but could improve the performance and ease of operation of the setup, whereas constraints are real-world restrictions and boundaries around which the setup must be designed and developed.

### 3.1.1 Requirements

- The test setup allows handling of liquid (e.g. diesel) fuels.
- The test setup is able to measure momentum flow rate  $\dot{M}$  and mass flow rate  $\dot{m}$  of the injected fuel. The injector nozzle coefficients,  $C_d$ ,  $C_a$ ,  $C_v$ , and  $C_M$  can be determined using this data.
- The test setup can accommodate injections with solenoid energising times (ET) that are either short ( $ET \approx 10^{-4}$  seconds) or long ( $ET \approx 10^{-3}$  seconds), with sufficient temporal resolution. Inter-injection spacing events of  $t \approx 10^{-4}$  seconds are supported.
- The test setup must be safe to work with; a combination of high-pressure and flammable liquids/gases can pose a great danger to the health of the lab users.

### 3.1.2 Preferences

- Next to liquid fuels, the setup additionally allows the characterisation of gaseous fuels, such as hydrogen. The characteristics of both fuel types must be well understood to avoid conflicting behaviour during the experiments.
- Ambient conditions of the test cavity (i.a. gas composition,  $p$ ,  $T$ ) should be as close to typical in-cylinder conditions as possible to minimise systematic error. This would indicate the need for a pressure vessel to accommodate the measuring components of the setup.
- The test setup equipment ought to be kept as simple as possible. This ensures both good accessibility to the test cell and less need for instruction.
- The method of measuring is preferred to be as "direct" as possible; the required parameters are not obtained through e.g. integration or derivation since this can magnify the biases in the measured parameters.
- The setup is versatile enough to accommodate multiple injector designs without the need for a specialised holding apparatus for each injector design. Additionally, the setup allows for a wide variety of fuel injection parameters such as injection pressure and temperature.

- The test setup can accommodate both single and multi-hole injector designs. For multi-hole designs, distinction of measured parameters between individual holes is possible.
- The test setup induces low levels of interference noise in the sensors.

### 3.1.3 Constraints

- Although funding has been established, the budget is not unlimited.
- The test setup can only have a certain size, space within the ZEL (Zero Emission Lab) is not unlimited.
- In the aftermath of the initial COVID-19 pandemic, resources for manufacturing companies have become scarce, resulting in much longer than normal lead times. This must be taken into account when ordering raw materials and products.

## 3.2 Measurement methods

Experimental FIE characterisation depends on an appropriate measurement technique for accurately measuring the requested characterisation parameter. Although optical-based measurement setups have allowed Cheng et al. [25], Zhu et al. [26], and Payri et al. [27] to effectively qualify the injector performance, they rely heavily on spray model correlations and are therefore not completely suitable for accurate quantitative measuring. For measuring the two most important injection characterisation parameters, the mass- and momentum flow rate, a multitude of measurement techniques exist that can be positioned into either the former or the latter based category. In the mass flow based category, the two most widely used concepts are the Bosch and Zeuch rate of injection (ROI) methods [6]. In the momentum flow based category, this is the jet impingement force method [20, 7, 28]. These three measurement techniques will be discussed in the following paragraphs.

### 3.2.1 Bosch rate of injection method

The Bosch ROI method, originally developed by Wilhelm Bosch in 1966, consists of a relatively long fuel-filled tube in which fuel is injected [29]. The injection creates a propagating dynamic pressure wave inside the tube, from which the nozzle velocity and thus mass flow rate can be derived. This holds only for quasi-unidirectional flow, however, indicating that the method is not suitable for multi-hole injector types; the nozzles that spray fuel towards the tube wall might induce extra friction effects. The strain gauge that measures the dynamic pressure is placed directly next to the injector nozzle, to minimise signal lag. An adjustable orifice plate that is placed after the measuring tube causes the initial pressure wave to reflect back towards the injector nozzle. The time between the initial and reflected pressure wave allows calculation of the speed of sound inside the fuel medium. As a means of damping out the pressure waves inside the measuring tube, a following tube is placed after the measuring tube that works in cohesion with the adjustable orifice plate to tune the speed of damping. Finally, a check valve enables collection of fuel and restores initial static pressure in the system.

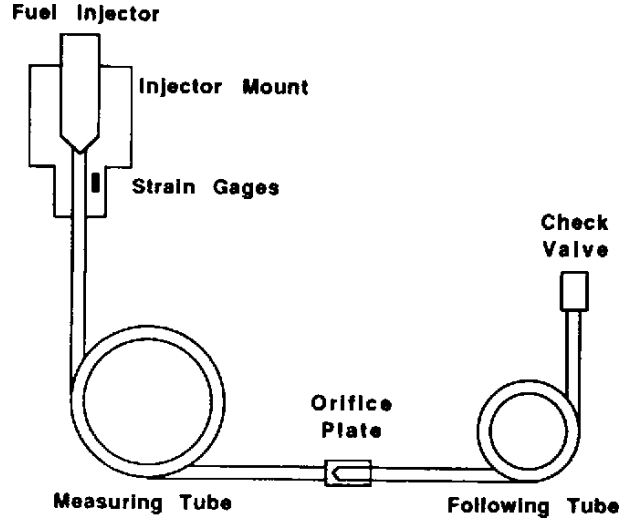


Figure 3.1: Schematic of Bosch ROI device [6]

When the injector nozzle is positioned such that the spray axis is quasi-parallel to the measuring tube the dynamic pressure is given by [6]

$$p = c \cdot \rho \cdot v, \quad (22)$$

where  $c$  [m/s] is the speed of sound in the medium,  $\rho$  [kg/m<sup>3</sup>] the density of the medium and  $v$  [m/s] the fluid velocity. If Equation 22 is combined with the continuity equation the mass flow rate can be derived as a function of the dynamic pressure  $p$ :

$$\frac{dQ}{dt} = \frac{A \cdot p}{c \cdot \rho} \rightarrow \dot{m} = \frac{A \cdot p}{c}. \quad (23)$$

From Equation 23 it is clear that no knowledge about the fluid conditions (such as fluid density and compressibility) inside the measuring tube is necessary for the mass flow measurement. Other characteristics of this measuring method can be listed as follows.

- Applicable to measuring of gas ROI, as i.a. compressibility is captured in the measured speed of sound  $c$  in the medium.
- Sufficient measuring tube length is needed for “finite” measurement of reflected pressure wave timing.
- Unsuitable to closely spaced, multiple injections. As a result of the reflected pressure waves, the system needs a certain amount of time to return to initial steady state conditions.
- Without extensive modifications of the apparatus, only applicable to single hole injector types.
- Fuel is injected into an identical medium. This does not allow replication of in-cylinder conditions.

In an attempt to circumvent the limitations of the Bosch ROI method concerning multi-hole injector types, Marcic developed an apparatus capable of measuring mass flow rates for individual injector nozzle holes, based on the same pressure wave principle as the



Bosch method [30]. Rather than injecting into a long fuel filled tube, every injector hole injects into separate fuel-filled measurement chambers. Assuming that the nozzle axis is aligned to the chamber axis, Equation 23 can similarly be used to determine the mass flow rate, albeit for individual nozzle orifices. The method uses a combination of deformation membranes in a Wheatstone bridge as the means of measuring chamber pressure, temperature compensated due to the Wheatstone bridge. Unlike in the Bosch method, an additional experiment must be carried out to determine the speed of sound inside the medium. Additionally, the largest disadvantage of the method proposed by Marcic is that every unique injector design requires a new, separate measurement apparatus.

### 3.2.2 Zeuch rate of injection method

Similarly to the Bosch ROI method, the Zeuch ROI method also focuses on measuring mass flow rate. This technique makes use of a constant volume chamber filled with fuel. The chamber pressure rises when fuel mass is injected into the control volume. The mass flow rate from the injector is linked to the derivative of the chamber pressure  $p$  [Pa]:

$$\dot{m} = \frac{\rho \cdot V}{K} \frac{dp}{dt}, \quad (24)$$

where  $\rho$  [kg/m<sup>3</sup>],  $K$  [Pa N/m<sup>2</sup>], and  $V$  [m<sup>3</sup>] are the fuel density, fuel compressibility, and volume of the chamber, respectively. In contrast to the Bosch ROI method, the Zeuch chamber relies on the accurate determination of the fluid properties— $\rho$  and  $K$ —inside the apparatus. To determine these parameters, a temperature probe is included in the setup. Secondary experiments have to be conducted to acquire  $\rho$  and  $K$  as function of  $p$  and  $T$ , nevertheless. Alternatively, these values can be found in literature or predicted using estimation methods. After the injection event has finished the solenoid relief valve opens and the chamber pressure quickly returns to the initial back pressure, controlled by a check valve. The fast acting valve enables the system to return to initial conditions much quicker than the Bosch ROI method, therefore allowing for more and shorter dwell timing in between injections.

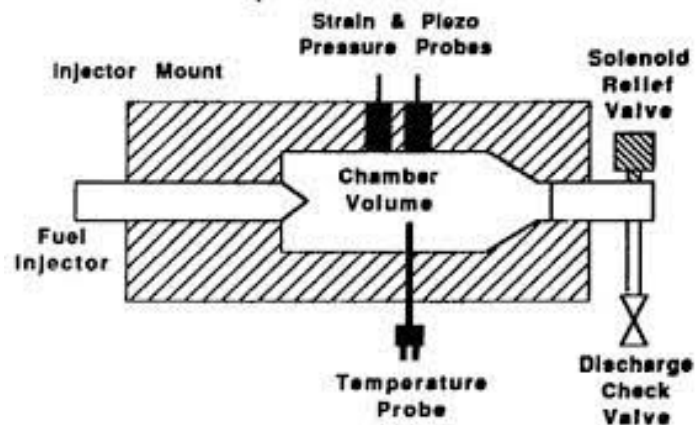


Figure 3.2: Schematic of Zeuch ROI device [6]

The pressure rise that results from the fuel injection induces a pressure wave into the Zeuch chamber. The design of the chamber must account for this, effectively limiting the propagation of the pressure waves such that measurement noise is minimised. The same

applies to the positioning of the pressure sensors. For the pressure sensing, generally a strain type sensor is used in conjunction with a piezo type sensor. The former has limited dynamic response but does not suffer from drift, whilst the latter is characterised by the opposite phenomena; the combination offers a workaround solution. Characteristics of this measurement method are as follows.

- Total injected mass follows directly from measured pressure, unlike the Bosch ROI where the signal must be integrated over time. However, the signal itself is generally more noisy than that of the Bosch method [6].
- Generally more compact space-wise than the Bosch ROI technique.
- Not suited for characterisation of individual injector holes, as all holes are placed in the same control volume chamber.
- More suited to closely-spaced injections than the Bosch ROI method.
- Fuel is injected into an identical medium. This does not allow replication of in-cylinder conditions.
- Secondary experiments, literature, or correlations are needed since accurate fluid properties inside the chamber are necessary for proper determination of the mass flow rate.

### 3.2.3 Jet impingement force method

The Bosch and Zeuch characterisation technique are only applicable to determining injector mass flow rates. For the determination of the rate of momentum flow (ROM) a separate technique is necessary. The most common technique found in literature is the jet impingement force method [20, 7, 28]. It is based on the observation that an external force vector applied to an object or control volume will change its linear momentum. The integrated force over a time interval (equal to the impulse  $J$  [kg·m/s]) is equal to the change of momentum over that same interval:

$$\int_{\Delta t} \vec{F} dt = \vec{J} = \Delta \vec{M}. \quad (25)$$

Hence, the magnitude of the force vector  $\vec{F}$  is identical to the rate of momentum change  $\dot{M}$  in the same direction as the force vector. If the flow velocity along a specific axis is reduced by impingement of the flow, the force that is required for the impingement is directly correlated to the momentum flow rate on that same axis. Figure 3.3 shows a schematic of an impingement setup for fuel sprays. If the assumption is made that the spray is uni-axial in horizontal direction, then the force measured by the sensor is identical to the momentum flow rate of the flow. This is only the case if the sensor is mounted perpendicular to the flow direction, and if the residual velocity in the direction of the spray axis is zero. A jet impingement setup is also able to measure the momentum flow rate of a multi-hole type injector, provided that adequate spacing between individual jets is assured. The geometry of the sensor target plays a large role in this; if the target is too large or placed too close to the nozzle exit, the flow of other nozzles might interact with the spray and thus interfere with the momentum measurement. This is especially the case with gasoline injectors, as the umbrella angle between nozzle holes is generally

quite small.

Provided that the total injected mass of a single injection or set of injections can be measured, the jet impingement characterisation technique also allows the determination of hole-to-hole mass flow rate profiles. The approach for this possibility is discussed into more detail in section 4.5. General characteristics of the jet impingement momentum flow rate measurement technique include:

- Capable of directly measuring hole-to-hole momentum flow rate.
- Placement and geometry of the impingement target are critical.
- Versatile since the injector unit is not directly connected to the measurement apparatus.
- Since the ambient medium can be (pressurised) air, in-cylinder conditions can be replicated.
- More suited to short, closely spaced injections than the Bosch ROI method. Limiting factor is the transient behaviour of the injector, not the measurement apparatus.

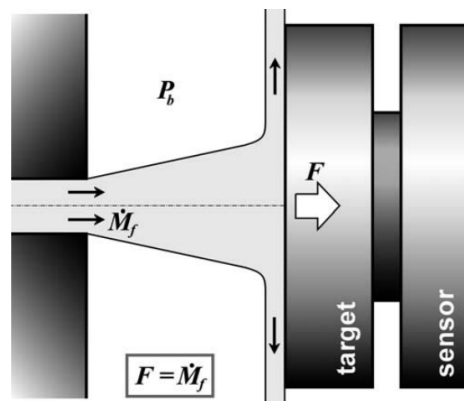


Figure 3.3: Schematic of jet impingement force method [7]

### 3.2.4 Commercial solutions

For the Bosch and Zeuch ROI method, several commercial options are available for purchase. IAV Automotive Engineering for example, offers the IAV Cross; based on the Bosch measuring technique it is able to characterise shot-to-shot mass flow rate of multi-hole injectors. It offers solutions for both gaseous and liquid fuels, ranging in cost for a full test bench from approximately €500.000 to €900.000. In contrast, the measuring tool as offered by Moehwald GmbH uses the Zeuch principle. By making use of a dedicated ultrasonic sensor, they are able to directly measure the speed of sound in the medium. Therefore, it is not depending on accurate determination of the fluid density and compressibility. Their solutions range in cost from €60.000 for a 500mg/cycle maximum injection size to €130.000 for a 25000mg/cycle maximum injection size. Note that these prices are for the measuring apparatus only; a full test setup ranges from €300.000 to €1.000.000 accordingly.

At the moment, the absence of a dedicated injector parameter measurement setup



prevents the researchers within the Power & Flow group from experimentally characterising fuel injectors. The group has therefore allocated a certain budget for the purchase or development of an experimental setup that is able to measure these spray parameters. Realistically, a research laboratory often requires specific options and needs for its measuring equipment, which can sometimes not be provided for by commercial equipment manufacturers. Combined with the relatively high costs associated with commercial solutions, the decision is made to fully develop the characterisation setup in-house at the TU/e. It is more feasible to develop an in-house dedicated unit that can be specifically formed to the requirements imposed by the Power & Flow research group.

### 3.3 Method selection

With help of the RPC list, the suitability of each of the main measurement methods can be described and evaluated through a number of properties and measurement capabilities. These are listed in Table 1: note that the pluses and minuses indicate a *relative* qualitative characteristic and therefore indicate the suitability of a particular measurement method for that capability. In essence, “- -” indicates a low level of suitability whilst on the other side of the spectrum “++” indicates a high level of suitability. As indicated in the table, all three main measurement methods can be used for the determination of injector mass flow rate. Whilst the Bosch and Zeuch method can do this directly, the impingement method relies on the scaling of the momentum flow rate with the cumulative injected mass. Hence, an additional experiment is necessary for the determination of the cumulative injected mass. For liquid fluids the injected fuel can be collected relatively easily and weighed directly. For gaseous fluids, an alternative method must be sought after. With the Bosch method, the cumulative mass also cannot be directly determined but it can be obtained via integration of the mass flow rate signal.

In contrast, the Zeuch method links directly to the cumulative injected mass. For transient injections the Bosch method is preferred since it inherits a “smoother” signal [6], and does not need a software-controlled relief valve as is the case with the Zeuch method. Both the Bosch and Zeuch method however, can sometimes show a small negative “spike” at the start of the initial rise in the pressure signal, which can increase the difficulty of determining the start of injection. The signal rise is much clearer observed in the impingement technique, although a certain time delay between actual and measured start (and end) of injection must be taken into account since a certain distance between the injector tip and measurement sensor is always present. In the Bosch method, this time delay is also present because the pressure sensor generally cannot be mounted directly next to the injector tip.

Table 1: Properties and measurement capabilities for main measurement methods

Capability/property	Bosch long tube	Zeuch chamber	Impingement force
<b>Mass flow rate</b>	Yes	Yes	Via additional experiment
Steady state	+	+	+-
Transient	+	+	+-
<b>Momentum flow rate</b>	No	No	Yes
Steady state	--	--	++
Transient	--	--	++
Spatial measurement	--	--	--
In-cylinder replication	--	--	+
Individual hole capability	--	--	+
Measurement noise	+	-	+
Simplicity of setup	+	-	+
Versatility for injector types	+	+	+

Momentum flow rate can only be measured by the impingement method. This means that this is the only measurement method that allows for the calculation of not just  $C_d$ , but also  $C_v$ ,  $C_a$ , and  $C_M$ . Additionally, the impingement method is the only method capable of accurately replicating in-cylinder conditions if necessary, and can determine nozzle conditions for individual injector holes whereas the other two methods can only determine injector-averaged parameters. The Bosch and impingement technique arguably are the most suitable measurement methods in terms of simplicity of the experimental setup: both techniques only require either one pressure or force sensor and no other components, whereas the Zeuch method requires implementation of a fast-acting relief valve and additional detailed knowledge of fluid properties. However, for the impingement method accurate alignment between the injector and force sensor is required. For accurate alignment of the force sensor to the injector hole, either the injector or the force sensor must be able to rotate and translate over multiple axes. This is especially important in single-hole injector types with off-axis nozzles or multi-hole injectors, where the sensor axis is not placed axially to the injector body length axis.

With the impingement method, the potential systematic and random errors that are prevalent in the momentum flow measurement are carried over to the mass flow rate signal. This potential uncertainty can only be validated by performing the same experiment with either a Bosch or Zeuch ROI device. Another uncertainty is in the measuring of the total injected mass, which traditionally has been done by collecting the injected fuel and weighing it with scientific scales [31, 32, 33]. These scales have a limited accuracy that might impact the weighing accuracy of the retrieved fuel sample. Furthermore, the evaporation of the injected fuel—not only in the fuel spray but also in the collection cup during the weighing process—can underestimate the measured weight of the fuel sample [34].

From the RPC’s and performance indicators of Table 1, the conclusion is made that the jet impingement force method is the key candidate for developing into a concrete setup design, following additional functionality criteria. The following section will discuss the required system capabilities and relevant physical component design aspects that are necessary for evolving the measurement concept into a fully functioning physical setup.

# 4 Experimental setup design

In the previous section, based on the relevant RPC's and measuring method properties, the jet impingement force method was selected as the most promising method for further development. In this section, the required functionalities of the measurement setup are introduced, as well as the components needed to ensure proper fulfilment of these functionalities.

## 4.1 System overview

The main purpose of the setup is the characterisation of fuel injectors via the acquisition of momentum flow rate and, secondly, injected mass quantity. There are a number of secondary functionalities that allow the characterisation to proceed. Both kinds can be characterised by:

- *Delivery of pressurised fuel to the injector*  
Clean, particulate-free pressurised fuel must be delivered to the injector at an adequate rate. The fuel must be filtered to prevent particulates from damaging the intricate injector. The fuel pressure must be kept as constant as possible throughout the injection, and the pressurisation of the fuel should introduce as little additional heat as possible to the fuel sample as this can influence the fuel flow, and thus the injector behaviour.
- *Stability of boundary conditions in the impingement apparatus*  
Ambient conditions in the impingement apparatus must be kept as stable as possible; changes in ambient temperature and pressure can have a non-negligible impact on the measurement. Turbulent airflow might disturb the fuel spray. The sensor axis must be correctly aligned to the spray axis. The diameter of the spray target and the distance between the target and injector nozzle must be chosen such that the entire spray—and only that spray—is captured by the momentum sensing equipment.
- *Control of the fuel injector solenoid*  
The injector solenoid must be energised with high resolution, in the order of  $\mu\text{s}$ . The profile of the actuation current must be constructed such that the specification of the injector manufacturer is followed. This prevents solenoid burn-through for long quasi-static injections.
- *Accurate and precise measuring of the required parameters*  
Data acquisition between the various sensing and control parameters must be synchronised, hence being measured both in time and magnitude. The sensor choice for measuring the momentum is vital; all (dis)advantages of the various sensor types applicable for the measuring of the spray momentum must be understood before a sensor type is selected. All factors that might deteriorate the sensed signals must be well understood and mapped.

For the realisation of the required system functionalities a number of physical components are needed. The positioning of the components in the experimental setup can be captured in a Piping and Instrumentation Diagram (P&ID). Although the main functionalities are the same for the liquid and gaseous fuel experimental setup, a portion of the components needed to realise the functionalities are not shared between them. In Figure 4.1, the P&ID

for the proposed liquid fuel setup is schematised. Note the distinction between low- and high-pressure fuel lines, and control- and measurement signals.

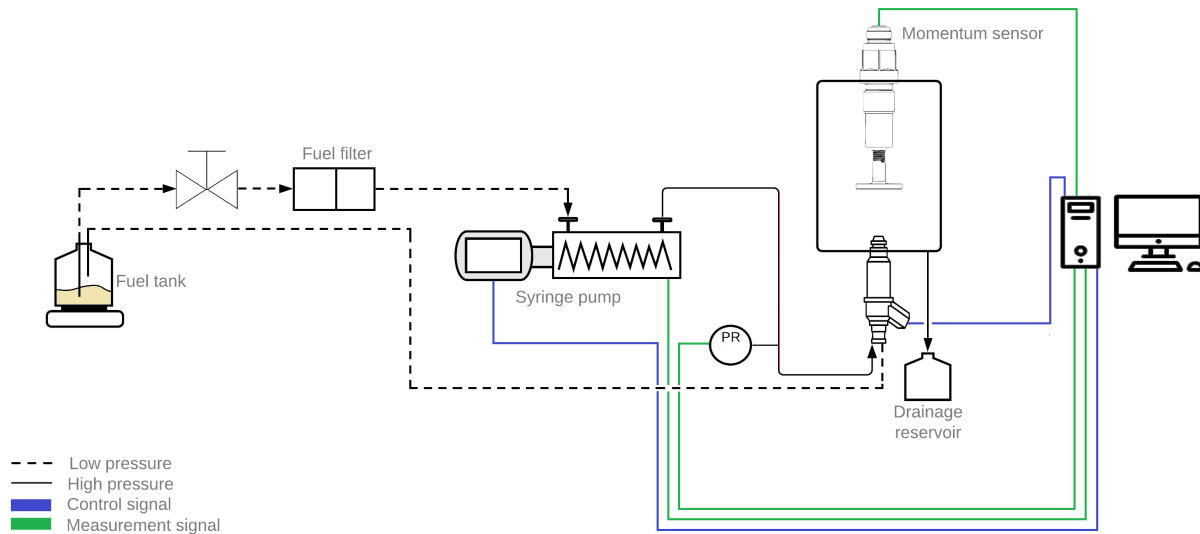


Figure 4.1: Schematic of the experimental setup designed for liquid fuels

## 4.2 Fuel delivery system

The experimental setup is not designed as a sub-part of an existing setup at the TU/e lab, indicating that the design of all separate required components must be contemplated. For visualisation of the component's position within the experimental setup, please refer back to Figure 4.1.

### 4.2.1 Fuel storage and filtration

The design of the most upstream component of the fuel delivery sub-system, the fuel tank, must consider the impact of the component on both the safety and performance of the setup. The material of the fuel tank can either be glass or AISI 316L stainless steel alloy, to ensure that the (possibly corrosive) fuel will not react with the tank material. A glass 1 liter Erlenmeyer flask is chosen as it is cheaper than a stainless fuel tank with comparable dimensions and has the advantage of being transparent, therefore allowing the operator of the experimental setup to visually inspect the fuel in the flask. The conical neck of the Erlenmeyer flask will decrease fuel evaporation losses compared to a standard glass beaker. The conical neck causes a non-linear contact area of the fuel to the ambient air as the fuel level drops, however. This might cause non-linear fuel evaporation behaviour; the rate of evaporation must therefore be measured at multiple fuel levels in order to determine a fuel evaporation rate curve as function of fuel level in the flask. Minimisation of fuel evaporation is paramount (see section 4.5), but typically cannot be prevented completely. A Teflon plug is designed to be placed over the neck of the flask, in order to minimise the rate of evaporation of the fuel from the flask. The fuel pickup and return line are routed through the plug into the flask, and a small vent hole is added such that the pressure in the tank does not drop below atmospheric pressure by removal of fuel volume during injection events. The inlet of the pickup is situated slightly above the bottom of the Erlenmeyer flask such that unwanted impurities that deposit on the bottom of the tank are less likely to flow to the injector. Additionally, if the density of the tested fuel is lower



than the density of water any traces of water in the fuel will also be kept from entering the system. Water is an unwanted impurity because it has no lubricating properties and can therefore cause damage to the high-pressure pump (depending on the type of pump) and injector internals. The second type of impurities are abrasive particles, which can wear out pump components and if large enough block injector internals. In the rare event that abrasive particles do enter the fuel pickup line, a fine 2  $\mu\text{m}$  particulate filter placed after the fuel tank prevents the particles from flowing to the downstream components. Whilst commercial vehicle fuel systems often incorporate separate coarse and fine fuel filters to prevent clogging of the fine filter, within this setup it is deemed unnecessary since the expected fuel throughput in the setup is relatively low.

An important point to consider is the effect of the Teflon plug on the performance of the weighing scales. It must be positioned such a way that at any point in time neither the fuel lines and the Erlenmeyer flask simultaneously touch the plug. Otherwise, the measurement might be affected by stiction or torsional effects that overestimate the fuel weight that is left in the fuel flask and therefore causes an underestimation of the consumed fuel mass.

The chosen flask volume is dictated by three main factors. Firstly, the heat capacity of the fuel is directly correlated to the flask volume. Depending on the desired injection pressure and pressure pump type, the temperature of the return flow from the pump and injector flowing back to the fuel flask can be high enough for the fuel in the flask to heat up, and thus changing the flow properties. Fuel coolers that add unwanted complexity can be added to the fuel return lines, or the heat capacity of the flask can simply be increased by enlarging its dimensions. Secondly, the flask volume indirectly dictates the maximum achievable resolution of the Sartorius<sup>®</sup> Secura<sup>®</sup> 5102-1s scientific scales used in the determination of the total mass of the injected fuel. These scales have a certified resolution of  $10^{-5}$  kg. To minimise the effect of the scales' maximum resolution on the accuracy of the measured total mass by using an adequately large enough number of injections, the volume of the fuel flask must be large enough to accommodate this amount of injections. The third factor is the draining of the fuel system when a different fuel or fuel blend must be tested. Using an adequately large fuel flask, draining of the system can be carried out more conveniently because fuel only has to be refilled once. However, one must consider that a large fuel system is considered disadvantageous when a small-batch or expensive fuel sample is to be tested.

#### 4.2.2 High-pressure pump

As discussed in section 2.2, contemporary DI diesel engines typically implement common rail injection systems. In heavy-duty systems, the high-pressure pump is generally driven by a camshaft mounted directly to the engine. In light-duty systems, the pump is usually a standalone unit driven by either the generator belt or dedicated V-belt. Such a standalone unit is therefore more suitable to be implemented in an experimental setup. Moreover, the single injector in the experimental setup requires only a fraction of the maximum flow rate of a heavy-duty pump. Propulsion of the light-duty pump can easily be resolved by coupling the pump to an electric motor. Both types incorporate cam lobes and plungers to generate pressure. The number of cam lobes directly correlates to the number of pump strokes and hence number of pressure pulses in a single four-stroke cycle. Due to practical reasons the number of cam lobes and thus pressure pulses is limited, which can introduce

a harmonic oscillatory behaviour in the rail pressure despite the damping of the common rail fuel volume.

In the Eindhoven High-Pressure Cell (EHPC) combustion vessel, situated at the Eindhoven University of Technology, a similar plunger pump is used to generate pressure in the rail. Although the pump is not driven by an electric motor but by compressed air, the same pulsating pressure effect is observed in this setup. Contrary to a combustion engine where there is a timing correlation between the pump strokes and TDC (and therefore indirectly the injection timing at a given load point), the EHPC and other similar setups display no synchronisation between injection timing and high-pressure pump plunger position in its stroke. Rather, the time of injection is only governed by the ambient conditions in the combustion vessel. Therefore, the actual rail pressure is a random value of the harmonic pressure trace at the moment of injection.

For overall pressure control in common rail systems, two main strategies appear:

- Supply more fuel than necessary to the common rail and install a pressure control valve (PCV) on the common rail to spill the excess fuel back to the fuel tank. Whilst being a relatively simple solution, this option results in a large, high-temperature return flow. Therefore, a dedicated cooling circuit is required to ensure a constant temperature of the fuel in the supply line.
- Meter the fuel flow at the high-pressure pump and adjust the pump speed such that only the necessary amount of fuel is supplied to the common rail. A common approach is to meter the pump inlet flow with an inlet meter valve (IMV). The main advantage of this strategy is the general avoidance of excess compression of fuel which would otherwise result in lower hydraulic performance and higher fuel temperatures, albeit at the cost for a more complex setup. In some cases, a PCV can be used to provide additional trimming of the rail pressure.

An alternative for the common rail high-pressure pump as described previously can be found in a linear pressure or syringe pump, which have previously been implemented successfully in comparable high-pressure fuel injection setups.[32, 35, 36]. The mechanism for pressure generation in a syringe pump relies on a linear stepper motor attached to a plunger that is mounted in a cylindrical sleeve. A valve in the inlet allows the plunger to fill the cylinder with fuel as the plunger moves to its bottom position via rotating the linear screw anti-clockwise. By closing the inlet valve, opening the outlet valve, and rotating the linear screw in clockwise direction the fuel in the outlet is pressurised. Since the majority of syringe pumps are only able to pump a limited cylinder volume before they must refill, sustaining continuous injection events over a long time period without interim refilling is difficult. Note that, however, there are some dual syringe pump systems that allow for continuous operation at a fixed pressure or flow.

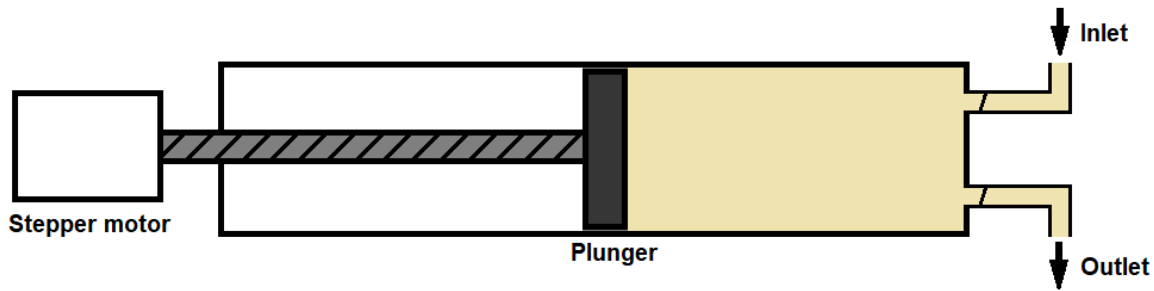


Figure 4.2: Schematic of syringe pump working principle

The pressure is controlled by incrementally moving the plunger position with the stepper motor. Via an internal control system, the pump can either be programmed for respectively constant or rate-shaped flow rate or pressure. The linear screw allows for very precise and linear pressure control, as the plunger position is a linear function of the stepper motor rotation. With the controller, the pressure can be held constant even under the influence of relatively small and high-frequency perturbations. The precise and fast pressure control ensures that no excess high-temperature pressurised fuel needs to be spilled back to the fuel tank, therefore helping to keep supply fuel at a constant temperature. Note that there will always be some return flow from the injector itself, that has a higher temperature than the supply fuel. Theoretically, there is no need for a common rail since the fuel volume situated inside the pump can act as the rail volume. A secondary advantage of the syringe pump system is the compatibility with exotic research fuels. The relative velocity and movement of the plunger are slow enough such that no additional lubrication between these components—which would normally be provided by the fuel’s own lubricity—is needed.

Given the substantial number of advantages compared to the high-pressure common rail pump, the choice was made to incorporate a Teledyne ISCO 100DX syringe pump into the design of the setup. Although this pump has a relatively low maximum pressure of 690 bar, it is viable as an initial step in demonstrating the proof concept, validating an adequate level of performance of syringe pumps in experimental fuel injection setups.

### 4.2.3 Fuel lines

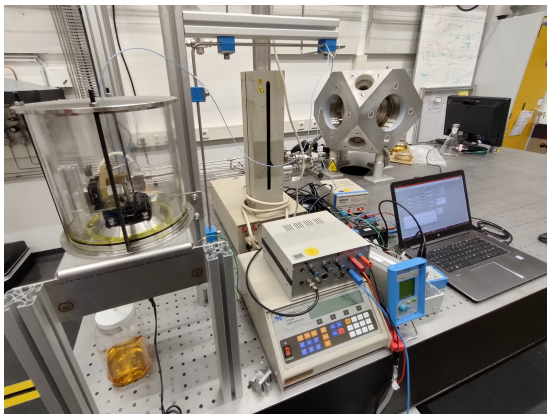
The fuel lines, depending on their position within the setup, must be able to withstand high pressures without mechanical breakdown and various (non-)corrosive fuel types, whilst allowing for high enough fuel flow rates. Upstream of the syringe pump, 1/4” Swagelok<sup>®</sup> AISI 316L stainless steel fuel lines are used with a maximum pressure rating of 710 bar. Because the connections to the 100DX pump are 1/8”, two reducing unions are used on both the up- and downstream side of the syringe pump. The AISI 316L alloy is chosen as this has previously shown excellent compatibility with a wide variety of fuel types. For the return fuel line coming from the injector, a semi-clear Teflon hose is used as this allows the operator to spot unwanted air bubbles in the fuel return line.

Ideally, specialised Swagelok<sup>®</sup> annealed AISI 316L high-pressure fuel lines are used, capable of withstanding fuel pressures of up to 2068 bar. Due to the present situation with extremely long lead times for certain components, the implementation of these specialised high-pressure lines was not yet possible. Therefore, downstream of the syringe pump the same 1/4” tubing is implemented. Due to further issues with the delivery of specialised

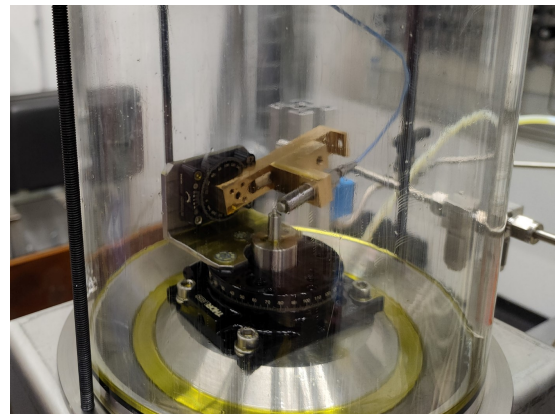
1/8" tubing that comprises the connections to the 1/8" fittings of the syringe pump, the maximum allowable pressure in the system is 590 bar, some 100 bar lower than the maximum delivery pressure of the current syringe pump. The expectation within the Power & Flow research group is that in the near future a 2000 bar syringe pump will be purchased that can replace the Teledyne ISCO 100DX pump, hence the need for such high-pressure rated lines. Since the syringe pump acts as both the high-pressure pump and common rail, a direct connection between the pump and injector is established via the high-pressure fuel line.

### 4.3 Injection chamber

The injection chamber, shown in Figures 4.3a and 4.3b, is the component of the experimental setup into which the fuel is injected. It houses the momentum sensor and injector, and separates the fuel residue from the environment. The injection chamber is built up from a base plate, PMMA "sleeve" and a lid, which are sealed by O-rings to prevent any fuel from leaking. The PMMA sleeve allows for visual inspection of the fuel injection but at the same time restricts the ability of pressurisation of the injection chamber, due to the limited strength of the PMMA. The proposed solution for chamber pressurisation consists of a thick metal sleeve, clamped to the base plate and sleeve lid with threaded rods, that replaces the PMMA sleeve. Visual inspection could be guaranteed by implementation of sapphire inspection windows. One point of consideration is the positioning of the momentum force sensor, which is discussed in Section 4.3.2. Although the ability to pressure the injection chamber is a definite advantage as it allows the replication of an in-cylinder pressure, it adds much more complexity into the injection chamber design. Moreover, the influence of the chamber pressure on the steady-state mass flow can be replicated by modifying the injection pressure, provided that no cavitation occurs. As shown by Garcíá [8], the steady-state mass flow is a linear function of the root of the pressure drop as long as cavitation does not occur.



(a) Complete setup



(b) Injection chamber

Figure 4.3: Overview of physical setup and injection chamber

#### 4.3.1 Injector mounting

The injector is mounted to the base plate from below via a custom adaptor that is unique to every injector. The use of custom adaptors for different injector design ensures that only a relatively small component needs to be manufactured, once a new type of injector is to



be characterised. In the present work, a Bosch CRIP2 injector with 7 evenly spaced holes with a diameter of 0.1 mm and an umbrella angle of  $152^\circ$  is used for determination of the desired mass- and momentum flow rate traces. Figure 4.4 shows how the Bosch injector is mounted to the base plate (red). The injector-specific adaptor (green) is mounted to the base plate, where a O-ring prevents any possible fuel leakages. A clamping plate (blue) fits tightly into two parallel flat slots of the injector body, and clamps the injector to the base plate via two M8 10.9 threaded rods. Because the injector body is mostly cylindrical, a light interference fit is machined such that the clamping plate and flat slots preserve identical alignment of spray axes to the momentum sensor axis when the injector is reassembled after disassembly.

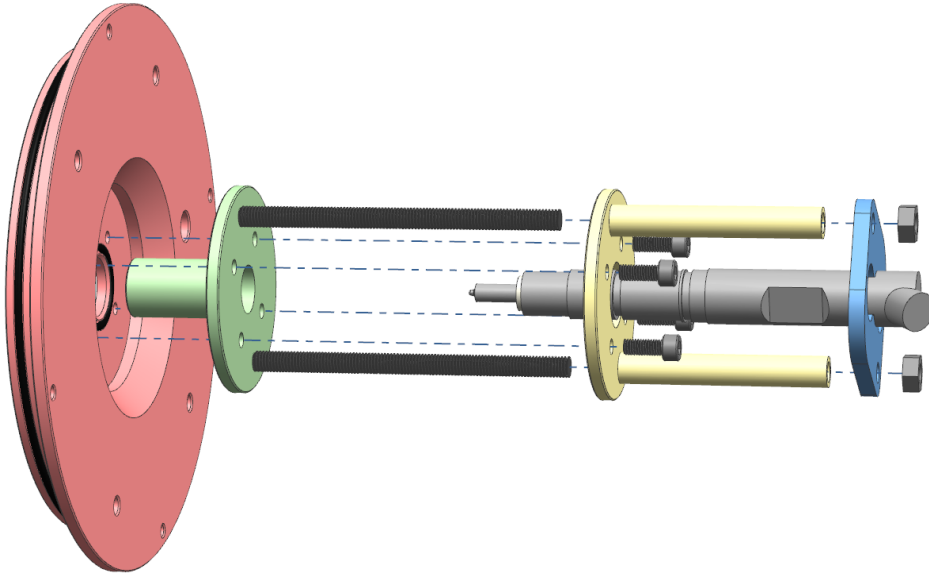


Figure 4.4: Exploded view of injector chamber base plate and injector clamp-down components

### 4.3.2 Sensor alignment

Accurate alignment of the momentum sensor is vital to ensure perpendicularity between the spray target and spray axis. Sufficient range of motion is required to allow sensor alignment with varying injector designs, ranging from single-hole (offset) injectors to multi-hole injectors with a large nozzle umbrella angle. The nozzles of the injector are oriented by the pitch of the holes and umbrella angle, depicted by the blue  $\theta$  and red  $\phi$  rotational axes in Figure 4.5. The momentum sensor can be positioned in the same rotation axes via Thorlabs *PR01/M* and *MSRP01/M* rotation stages with a maximum resolution of respectively 5 arcmin ( $0.083^\circ$ ) and 20 arcmin ( $0.33^\circ$ ). The expectation is that any possible misalignment will have a negligible influence on the measured momentum flow rate [34][8]. Following trigonometry, the error in the measured momentum flow rate due to sensor misalignment correlates with  $1 - \cos(\alpha)$ , where  $\alpha$  is the angle away from the spray axis. A brass bracket component allows translation of the sensor in Z-direction, such that the target-to-nozzle distance can be set with a set screw to 0.25 mm increments.

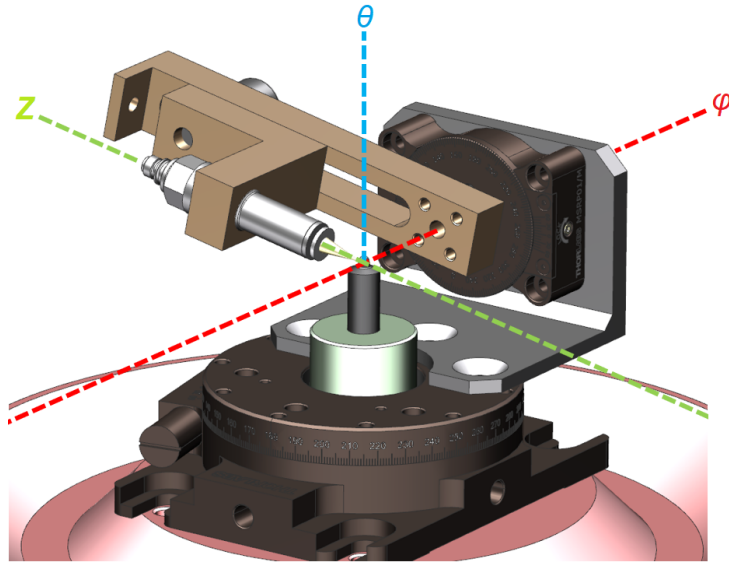


Figure 4.5: Schematic representation of the rotation and translation axes of the momentum sensor

In order to maintain a constant target-to-nozzle distance it is vital that the rotation axes of the sensor alignment fixture are coinciding with the centerline of the injector and injector tip, as depicted in Figure 4.6. If this is not the case for any of the two rotation axes, the sensor will describe an elliptical orbit around the injector resulting in a varying target-to-nozzle distance over the domain of movement. Note that in the current design, contrary to the work of Garcia [8], the injector is “fixed” in space with the sensor being aligned to the injector. This omits the need for an expensive flexible high-pressure fuel line as the fuel line fitting of the injector is always fixed in space. The disadvantage of this is that the PMMA sleeve and lid must be removed when the sensor alignment is adjusted.

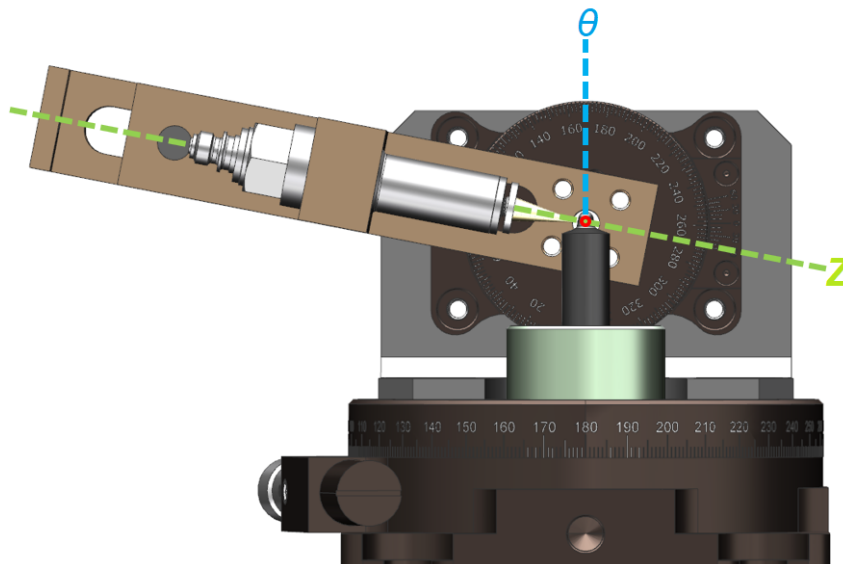


Figure 4.6: Schematic representation showing concentricity between the injector nozzles and alignment axes

## 4.4 Sensors

### 4.4.1 Rail pressure sensor

Whilst the syringe pump uses an internal sensor to control the system pressure, there is no option to log the reading with a data acquisition system. For this reason, a standalone piezoresistive Kistler 4067A5000 pressure sensor was installed in the high-pressure fuel line, at a distance of approximately 50 mm from the injector. The relatively close spacing between the sensor and injector ensures good temporal accuracy in measuring the propagation of pressure waves through the fuel line. A piezoresistive transducer is chosen over a piezoelectric transducer because an accurate quasi-static reading without signal drift is required. An additional benefit of the 4067A500 is the possibility to simultaneously measure temperatures in the 20 – 120 °C range.

### 4.4.2 Momentum sensor

For directly measuring the momentum flow rate of the fuel spray, the momentum sensor is undoubtedly the most important parameter. The characteristics of all relevant transducer and sensor types are analysed such that the best performing sensor for this particular application is selected. The applicability of each type of transducer can be expressed as a function of a number of requirements:

- *Ability to measure force*

The sensor must be able to measure the impingement force of the fuel jet. The type of sensor can be a force sensor to measure the force directly, or any other type of sensor based upon which the force can be derived..

- *Dynamic response*

The characteristic time of an injection is very short, indicating that a sensor with fast response time and adequate dynamic behaviour is required. Low sensor drift and a large discharge time constant are preferred. Additionally, because the initial impact of the fuel jet is violent, the eigenfrequency of the sensor should be adequately high.

- *Protection from high-stress impact*

The sensor internals should be protected from the spray impact via a sensor target fixture constructed out of an appropriate material. The high-pressure jet impacts on only a small area, indicating high stresses that the target must be able to withstand. An additional advantage of a spray target is that conduction of heat from the jet to the target can be reduced via the thermal properties of the material.

- *Tolerance to fuel*

The positioning of the sensor in the injection chamber can cause injected fuel, especially fuel mist, to come into contact with the sensor. This means that the sensor either supports prolonged contact with fuel, or protects the sensitive components from coming into contact with the fuel.

- *Future-proof sensor*

Although the sensor characteristics might be adequate for the current proposed experimental setup, potential influence of relevant future setup adaptations and improvements on the sensor choice must be considered such that longevity of sensor performance can be assured. One potential adaptation to the setup could be the

ability to pressurise the injection chamber, which will require a sensor that can handle these high pressures.

To measure the impingement force of the fuel spray, the most apparent option is a specialised force sensor. Alternatives exist however, such as the use of pressure sensors that are calibrated for measuring force instead of pressure. Initially, it is important to consider the different kinds of transducer types and their associated measuring characteristics. Among the appropriate transducer types are the following:

- *Piezoelectric transducer*

The piezoelectric effect is a phenomenon where an electrical charge is generated upon mechanical stress in certain materials. When it is subjected to a mechanical stress a direction-specific electrical polarisation occurs, resulting in an electrical charge difference on the surface of the material. With the help of an external charge amplifier, the output charge is conditioned to an output voltage that can be read by a data acquisition (DAQ) device. The cable that connects the transducer to the charge amplifier must be of a high-impedance type in order to minimise triboelectric noise that can otherwise have a detrimental effect on the charge signal. A sub-category of piezoelectric (PE) transducers is the integrated electronics piezoelectric (IEPE) transducer, where the conditioning electronics are mounted inside the sensor body as to avoid the need for an external charge amplifier. Hence, the main advantage of a IEPE-type transducer is the easier handling because it can use a standard cable to connect to a DAQ device. The drawback is the smaller flexibility in a laboratory environment, however: IEPE transducers always have a fixed pressure measuring range and relatively limited temperature range as well as only supporting dynamic, non-(quasi)static measurements. In contrast, PE transducers generally have a wide temperature operating range, adjustable pressure range, and capabilities for measuring quasi-static measurements. Truly static measurements are not possible, since the piezoelectric phenomenon induces a gradual charge loss over time [37]. In general, piezoelectric transducers (both PE- and IEPE-type) are used in applications where a good dynamic response is requested, due to their high eigenfrequency.

- *Piezoresistive transducer*

The piezoresistive effect implies that a change in electrical resistivity occurs when a mechanical strain is imposed on a semiconductor or metal. The change in resistivity results not only from conductivity change in the material, but also the geometry change as a result of the mechanical strain. Generally, for piezoresistive (PR) transducers, silicon-based semiconductor materials are used as their change in resistance is much more pronounced than for metals. Whilst the change in resistivity of a silicon-based resistor can be measured directly (i.e. a strain gauge), usually an arrangement of four resistors will be connected to form a Wheatstone bridge. The Wheatstone arrangement provides a much higher sensitivity than a strain gauge. In contrast to PE transducers, PR transducers are not suitable for dynamic measuring and should therefore only be used for static measurements. Unlike PE transducers, they do not display signal drift when a (quasi-)static load is applied.

Looking at the characteristics of both types of transducer and momentum sensor performance requirements, the piezoelectric transducer appears to be the more promising

choice. Important advantages over PR transducers to consider, are the better dynamic response and higher eigenfrequency. Although time discharge of the PE transducer prevents measuring static magnitudes, the timescale of an injection event is small enough to not affect the measurement. Since the drift is linear over time and not affected by outside parameters within the time span of an individual measurement, it can be compensated for in the post-processing since the measured force should be zero right before the start of injection takes place. Whilst an IEPE transducer might inherit less triboelectric noise, the limited flexibility for laboratory use severely limits its suitability as momentum sensor.

The main and most logical choice of sensor type for this particular application would be a PE force sensor since after all, the physical quantity to be measured is force. The most promising PE force sensor to appear in literature is the Kistler 9215A [32, 36, 38], capable of accurately measuring forces up to 200 N. The sensor combines a very high sensitivity with relatively high eigenfrequency and low temperature sensitivity. Whilst it is not acceleration-compensated and therefore has moderate axial acceleration sensitivity, Knox et al. show that the maximum error in the measured signal for this particular sensor is small [34]. Two other advantageous features are the small dimensions and addition of a mechanical thread in the pressure sensing face that can be used to mount a spray target to.

An alternative for the PE force sensor exists in the form of the PE pressure sensor, which also has seen use in several studies [34, 8]. Figure 4.7 illustrates that PE force and pressure sensors function in a similar manner, bar a diaphragm that is used in the pressure sensor to transform pressure into a mechanical strain. The difference in output lays in the calibration: force sensors are calibrated with respect to a known force and pressure sensors are calibrated with respect to a known pressure. Therefore, if the pressure sensor is calibrated with respect to force it will behave in similar fashion to a force sensor. If, in the near future, the Power & Flow research group decides to invest in a pressure sensors as opposed to a force sensor to measure the rate of momentum flow of the fuel spray, the reader can refer back to Appendix A for a general guideline on the proposed calibration process of a pressure sensor to measure force.

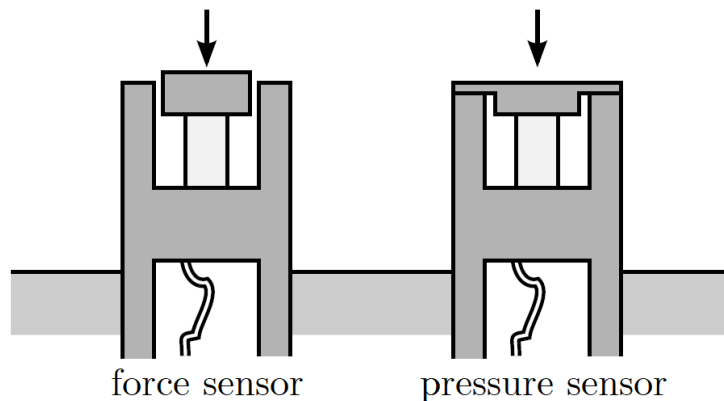


Figure 4.7: Differences in component layouts between PE force and pressure sensors. *Derived from [8]*

The diaphragm in the pressure sensor separates the pressure sensing piezocrystals from the injection chamber and therefore prevents contamination by the fuel, which is not the case for most force sensors. Although the spray target can be designed to shield the force sensing face from the majority of fuel particles, it cannot guarantee full protection. The



lack of a completely sealed sensing surface in the force sensor reveals a second potential issue: if the capabilities of the injection chamber are expanded in the future such that an in-cylinder pressure can be replicated by pressurisation of the chamber, the sensing elements will be exposed to the chamber pressure since the sensor (including wiring) is fully enclosed in the injection chamber. This will both introduce an unwanted zero point error as well as an unpredictable linearity of the sensor. Following future injection chamber design considerations and improvements, the sensitive parts of the pressure sensor will not be in contact with the chamber pressure and, therefore, they will not experience these unwanted effects. At the same time, the diaphragm prevents easy attachment of the spray target. Realistically, the only way to attach the spray target to the sensor diaphragm is by gluing with an appropriate adhesive. Another phenomenon to keep into account is a possible systematic error caused by the interaction of the spray target base and the sensor housing. If the diameter of the spray target base is too large with respect to the diameter of the sensor housing, a part of the impingement force is transferred—via the diaphragm flanks—to the sensor housing [34]. Simultaneously, a small base diameter complicates the process of attaching the spray target to the diaphragm.

For the current injection chamber a PE force sensor is the most appropriate momentum sensor choice. More specifically, the Kistler 9215A is selected as the most appropriate sensor for the setup. During the project, a meeting with a technical sales representative of Kistler Netherlands was held to discuss the choice for a force sensor in this particular application. They offered to hand over a Kistler 9217A demo force sensor on loan for the remainder of the graduation project, as an opportunity to demonstrate the proof of concept of the force sensor at zero costs. The sensor came included with a Kistler 5015A charge amplifier and 1631C high impedance cable. Unfortunately, at the time of writing, no 9215A demo sensor was available.

Table 2: Kistler 9215A and 9217A technical specifications [2]

	Calibrated 1% range [N]	Sensitivity [pC/N]	Axial acceleration sensitivity [N/g]	eigenfrequency [kHz]
Kistler 9215	0 ... 2	≈-95	<0.002	>50
Kistler 9217	0 ... 5	≈-105	<0.035	>20

As illustrated in Table 2, the characteristics of the sensors are similar, albeit in favour of the 9215A. The lower eigenfrequency of the 9217A might cause high-frequency perturbations in the measured signal, especially if the added weight of the spray target is taken into consideration. Assuming that the 9217A sensor can be described as a simple mass-spring system, the stiffness  $k$  [ $\text{N}\cdot\text{m}^{-1}$ ] is calculated following

$$k = 4\pi^2 f_n^2 \cdot m. \quad (26)$$

With a sensor weight of  $1.6 \cdot 10^{-2}$  kg, this gives a stiffness of  $2.52 \cdot 10^8$   $\text{N}\cdot\text{m}^{-1}$ . Depending on target diameter, the mass of the largest spray target (treated in section 4.4.3) is  $3.0 \cdot 10^{-4}$  kg. With Equation 26 and assuming identical stiffness, the theoretical eigenfrequency of the sensor plus spray target is determined to be 19.8 kHz. Given the fact that the borrowed 9217A sensor was a demo sensor with a relatively old calibration certificate dating from 2017 and the relevant sensor characteristics are worse than those of the 9215A sensor, the measured force signals might contain systematic and/or random errors. Therefore, one must take great caution in using the obtained force measurement traces in this report for **quantitative** analysis!

### 4.4.3 Spray target material and geometry

The impact of the fuel spray hitting the spray target can amount to a substantial mechanical stress. If the material of the spray target is not sufficiently able to withstand the repeated impact of fuel injections, mechanical pitting wear of the target face might occur. In case of pitting, the theoretical condition that the residual axial velocity of the spray must be equal to zero is no longer met, resulting in an overestimation of the momentum flow rate [39]. In order to select an appropriate material such that pitting or any other mechanical deformation is prevented, a derivation of the expected maximum encountered mechanical stress is presented. The derivation concerns a liquid jet with constant velocity and jet diameter. Whilst this is not coherent with reality, the assumption holds if the liquid vein of the spray impacts onto spray target. This depends on the liquid penetration depth and spray dispersion angle, which in turn depend on the pressure in the injection chamber [40]. Hence, an injection into a low ambient pressure environment conforms to this assumption. Conservation of momentum in the direction of the spray yields

$$\rho_f \cdot A_0 \cdot u_0^2 = A_0 \cdot \sigma, \quad (27)$$

where  $\sigma$  [Pa] denotes the mechanical stress on the spray target. By inserting the maximum theoretical spray velocity (Equation 1) into Equation 27, the stress can be described as a function of the injection pressure difference  $\Delta p$ :

$$\sigma = \rho_f \cdot u_0^2 = \rho_f \cdot \left( \sqrt{\frac{2\Delta p}{\rho_f}} \right)^2 = 2\Delta p. \quad (28)$$

In the current setup, with a maximum injection pressure of 69 MPa and maximum injection chamber pressure of 0.1 MPa, the maximum expected localised stress on the spray target will be approximately 136 MPa. If in the future the maximum injection pressure can be increased to 200 MPa the maximum stress will increase to 398 MPa. Hardness is the material property that defines the resistance to the maximum encountered stress of the liquid vein, as it is a measure of the resistance to localised plastic deformation. For this reason the spray targets are manufactured from AlMgSi1.0, a lightweight aluminium alloy with a high hardness (95 HV  $\approx$  315 MPa<sup>1</sup>). Foreseeing the higher expected wear of future higher-pressure injections, the impact surface of the target is further strengthened with a hard anodising treatment; a surface hardening treatment where a layer of very hard (1365 HV) aluminium oxide (Al<sub>2</sub>O<sub>3</sub>) of approximately 100  $\mu$ m thick is formed.

The geometry of the spray target must also be considered, as the fuel is ideally deflected into radial direction only. For this reason, a flat surface is considered for the spray target. A 3 mm metric thread on the backside of the target allows for easy mounting to the 9217A force sensor. In the design of the spray target, careful attention has been paid to keep the weight down as much as possible. Since the eigenfrequency of the sensor—assumed as a mass-spring system—is a function of the stiffness divided by mass, any additional weight of the sensor appendages is unwanted. For this reason, the thickness of the target surface and length of the mounting stem are minimised.

As depicted in Figure 4.8, three spray targets with differing face diameters have been manufactured. To capture the entirety of the fuel spray with the spray target and prevent underestimation of the momentum flow rate, the diameter must be adequately large.

---

<sup>1</sup>The Vickers hardness (unit [HV]) is used as a means of determining the hardness of a material, which can be expressed in ultimate tensile strength

The target-to-nozzle distance plays the same role in this regard: decreasing this distance generates an equal effect as increasing the diameter of the target. At the same time, there are certain characteristics that limit the maximum diameter of the target surface. If the diameter of the spray target is large enough, the sensor may experience external contributions from one or more of the neighbouring holes if a multi-hole injector is characterised. The contribution may consist of fuel from a neighbouring spray hitting the target, or turbulence effects from the entrainment process of a neighbouring spray. The diameter of the fuel spray at a certain distance from the injector nozzle can be estimated with the spray penetration model of Naber and Siebers [41], and can thus be used to determine the appropriate spray target diameter.

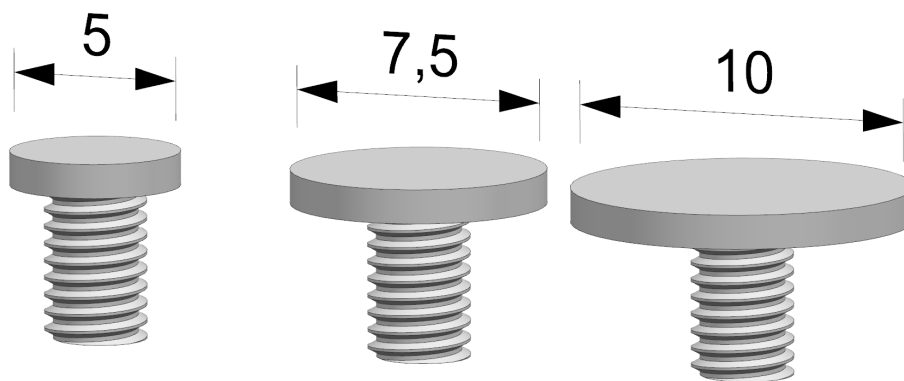


Figure 4.8: Geometry of selected spray targets with different face diameters. Depicted diameters in millimetres

A second factor that limits the diameter of the target is caused by entrainment effects of the spray. In the initial stage of the injection, the head of the spray is slowed down by the entrainment of air and drag. The deceleration causes an accumulation of fuel at the head of the spray and gives rise to a deceiving temporal shift and amplification of the measured momentum signal during the initial rise [42]. Simultaneously, behind the spray head, a low-pressure gaseous zone develops that causes a drop in measured momentum when it impacts the target. The influence of the (unrepresentative) low-pressure impact on the measured momentum flow rate can be decreased by choosing a spray target with smaller diameter, as this allows the low-pressure zone to pass around the target more freely. A more powerful solution is to decrease the target-to-nozzle distance, as this limits the level of entrainment and thus the magnitude of the developed low-pressure zone in the initial transient stage. Similar results can be achieved with a less dense ambient medium than air, e.g. helium. However, this will also affect the behaviour of the injector [36].

Postrioti et al. reason that both the optimum target-to-nozzle distance and target diameter are related to the type of injector used, injection pressure, ambient back pressure and spray dispersion angle. For diesel injections, they suggest a target diameter of approximately 7.5-15 mm and target-to-nozzle distance of approximately 5-10 mm which is in line with other work [32, 34, 38, 39]. A smaller target diameter of 5 mm is additionally selected as this might prove necessary for other injector designs.

#### 4.5 Momentum- to mass flow rate correlation

Whereas the jet impingement measurement technique is normally only used for the determination of the momentum flow rate, Cavicchi et al. show that it can also be used

to determine mass flow rate [32]. In fact, they show that hole-specific mass flow rates with good transient accuracy can be determined, a feature that the Bosch and Zeuch ROI method lack. With the assumption that the hole-specific contraction coefficient (denoted by the subscript  $i$ ) is identical to the mean contraction coefficient of the injector overall (denoted by the subscript  $tot$ ), it is determined via

$$C_{a,i} \approx C_{a,tot} \approx \frac{\sum \dot{m}_i^2}{\rho_f \cdot \sum A_{0,i} \cdot \sum \dot{M}_i}, \quad (29)$$

where the mass- and momentum flow rates represent values that correspond to the quasi-steady part of an injection. Substituting the result of Equation 29 into Equation 7 yields

$$\dot{m}_i = \sqrt{\rho_f \cdot C_{a,tot} \cdot A_{0,i} \cdot \dot{M}_i}. \quad (30)$$

This procedure requires the measurement of the steady-state mass flow rate of the whole nozzle, effectively necessitating a separate mass flow rate meter of the Zeuch or Bosch type. An alternative is found in the work of Naber and Siebers, and Payri et al., which only requires measurement of the total injected fuel mass [41][31]. Normalisation of the square root of the measured force output by the square root of the time-integrated output yields a profile proportional to the effective injection velocity:

$$u_{eff,i} \propto \sqrt{\frac{\dot{M}_i}{\int_0^t \dot{M}_i dt}}. \quad (31)$$

The product of Equation 31 and the independently measured total injected fuel mass per injection results in the mass flow rate profile of the  $i$ -th hole:

$$\dot{m}_i = \int_0^t \dot{m}_{tot} dt \cdot \sqrt{\frac{\dot{M}_i}{\int_0^t \dot{M}_i dt}} \quad (32)$$

In the current setup, the total injected fuel mass per injection is calculated upstream of the syringe pump by comparing the weight of the fuel in the fuel flask before and after the experiment and dividing it by the total number of injections, using the Sartorius weighing scales placed under the fuel flask. Payri et al. [42] show that measuring the fuel consumption upstream of the syringe pump yields similar results to measuring the injected fuel mass at the injector nozzle tip.

Before the experiment is started, it is of critical importance that an equilibrium position in the fuel system is achieved first. This implies properly bled fuel lines, a fully filled syringe pump (the pump-internal refill procedure ensures that the pump is always filled to the same maximum volume of fuel), and a fuel return line that contains no air bubbles. Any air bubbles that remain in the fuel system at the start of the experiment might skew the obtained fuel mass consumption value. After the injections are finished, the syringe pump must first be refilled before the fuel mass consumption value can be read from the weighing scales. In theory, the change in syringe pump volume multiplied by the fuel density could also be used to calculate the injected mass, but this would neglect any fuel return flow coming from the injector. Therefore, this approach would overestimate the actual injected fuel mass.

## 4.6 Data acquisition and injector actuation

For the acquisition of sensor data and actuation of the injector, a Virtual Instrument (VI) program has been developed in National Instruments' Labview™ software package. The GUI-based software package is based on the dataflow programming principle and allows for excellent software-to-measurement hardware integration. During normal use, the user will only be able to make changes to control parameters on the “front panel” user interface—depicted in Figure 4.9—ensuring that the block diagram structure remains unchanged. The hardware of the DAQ system is based on a NI 9174-cDAQ chassis, that allows installation of a variety of C-modules with various input or output capabilities.

The two main functionalities of the DAQ consist firstly of creating an appropriate actuation signal for the injector. The injector is controlled by an injector driver that turns a transistor-transistor-logic (TTL) digital input (DI) into an analog current profile specifically tuned for the injector. The energising time (ET) of the injection is governed by the length of the TTL-high ( $\approx 2 - 5$  V) signal, which is released from the DAQ device as an digital output (DO). Secondly, the DAQ device must be able to acquire the analog signals from the momentum-, rail pressure, and injector driver current sensors. A NI 9201 8-channel,  $\pm 10$ V, 12-Bit, 500 kS/s analog input (AI) module is assembled into the 9174 chassis to measure the analog signals. A NI 9402 4-channel, LVTTL (3.3V), digital I/O modules is used for the construction of the injector driver digital input signals.

On the front panel, the user can change all relevant injection properties, such as ET, injection frequency and number of injections of the main injection. The “down time” indicates the interval between main injections, whilst the “expected time” gives an estimate of the total experiment duration. A pre-injection can be initiated with a checkbox, and the ET and dwell time (DT) between the end of injection (EOI) and SOI of the main injection can be set. For logging the relevant data, the user can change the physical channels that are to be logged and set the sampling rate. Note that the current VI only supports single pre- and main injections, although the capability of performing post-injections can be added relatively easy. After every experiment, a text file is created that contains all relevant injections parameters for future reference. Furthermore, the user can choose to add notes or comments to this text file.

The generalised nodes that the created DAQ VI follows are visualised in Figure 4.10. Logically, the first step is to set the required injection parameters, as explained above. Next, the VI is initiated using the “run” button. The VI incorporates a custom block node to create a train of DO pulses that are sent to the injector driver, with the characteristics of the pulse train depending on the ET, injection frequency and number of injections. With Labview™ it is not possible to internally mix two pulse trains with differing TTL-high duration, time delay and duty-cycle, and send these over the same output channel. In the case of a pre-injection requirement, the VI overcomes this issue by creating separate TTL pulse trains that are sent over separate output channels and physically mixed using a hardware signal combiner. If a pre-injection is used, a time delay equal to the dwell timing plus pre-injection ET, is incorporated into the main injection pulse train, ensuring that the DO pulse is sent *after* the pulse train is triggered.

A second issue is the time synchronisation between the two pulse trains which, due to the dataflow principle and hardware limitations of the 9174 chassis, is difficult to realise. This is solved by adding an internal synchronisation mechanism that is crucial in ensuring that the two pulse trains are sent to the injector driver with precise dwell timing. The mechanism is based on a separate digital frequency pulse train that serves as an internal reference signal. The two TTL pulse trains are simultaneously triggered using two digital



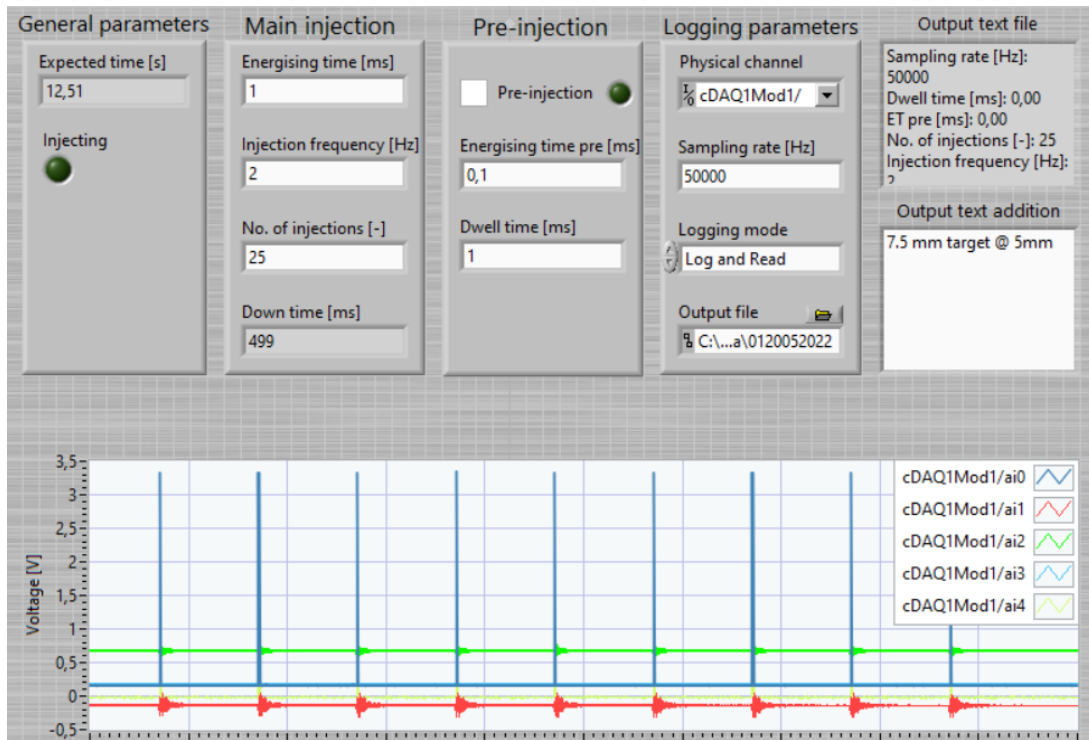


Figure 4.9: Labview™ front panel of developed DAQ VI

rising edge start triggers that act on the reference frequency pulse train.

When the “START” button is pressed, the VI will try to simultaneously initiate the logging of the AI signals and release of the DO pulse train, since this would time-synchronise the physical SOI to the start of data logging. The synchronisation mechanism as described above is only capable of synchronising digital outputs, indicating that a synchronisation error will remain between the DO and AI signals due to the limitations of the dataflow principle and cDAQ chassis. This synchronisation error is removed during post-processing.

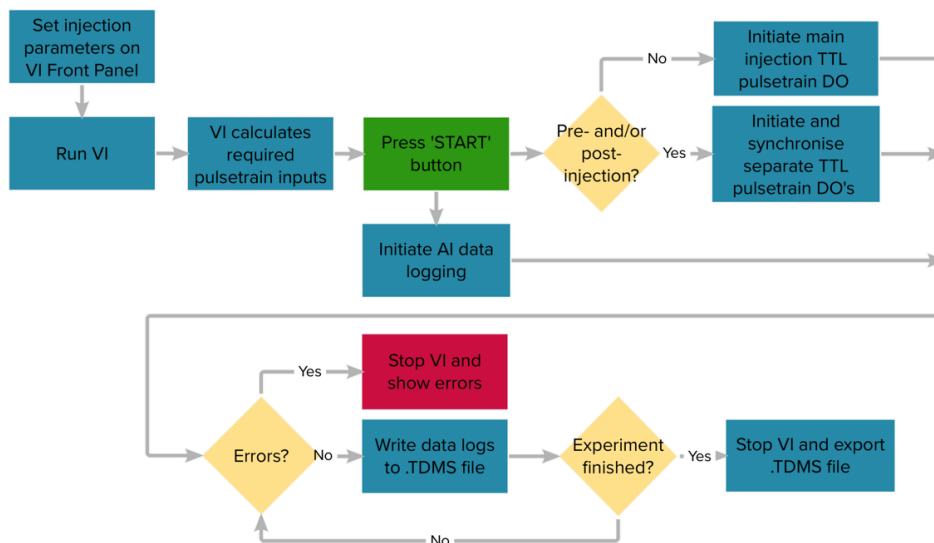


Figure 4.10: Schematic visualising the dataflow in the developed Labview™ DAQ VI

The total duration of the data logging is governed by the injection frequency multiplied by the number of injections, and an extra timed delay to ensure that the spray impingement of the last injection is fully captured. If no errors occurred, a .TDMS file containing all relevant measurement data is exported after the final injection, ready to be post-processed. If an error in the VI is encountered during the experiment, the VI is terminated immediately and an error report is sent to the user.

## 4.7 Implementation of gaseous hydrogen injections

One of the initial goals of the project was the implementation of both liquid and gaseous fuel injections in the experimental setup. Relatively early in the design process the focus was shifted to the implementation of liquid fuel injections only, as time constraints prevented both design and manufacturing of the specific components necessary for gaseous hydrogen injections. Generally however, the specific requirements have been taken into account in the design phase for the general setup components. As an example, the material choices for the fuel lines and injection chamber components have excellent resistance to hydrogen embrittlement. The choice of measurement concept should in theory also be suitable to hydrogen injections. Furthermore, the existing fuel lines can be connected to a pressurised hydrogen gas cylinder with a double-stage gas pressure regulator that can ensure constant pressure for the entire duration of experiments. The two main bottlenecks that currently remain are the measurement of the injected fuel mass and the disposal of the hydrogen gas, given that it can be a highly explosive substance when mixed with air in the right proportions. If very small amounts of hydrogen are injected, it may be vented directly through the ventilation system of the ZEL. If a risk of explosion exists due to increasing hydrogen amounts, however, aftertreatment in the form of combustion or chemical conversion might be necessary. As an alternative, the injection chamber could be filled with a non-explosive gas, such as nitrogen. To completely eliminate the explosion hazard, however, the complete ventilation system should in that case be filled with the same non-explosive gas.

For measuring the injected hydrogen fuel mass, future developers of the setup might consider a Coriolis mass flow meter. The maximum possible sampling frequency of said mass flow meter type is generally much lower than the timescale of an injection, however, which might cause issues in accurately measuring the mass flow. Therefore, a buffer vessel might need to be implemented in to the fuel system such that the mass flow meter can sense a more “steady” signal. In that case, the reader should adhere to the method for determining the nozzle hole mass flow rate as described by Cavicchi et al. in section 4.5. An alternative for a Coriolis meter might be the hydrogen injection chamber that is currently being developed by Doctoral candidate Max Peters at the ZEL. The chamber, already housing a in-chamber pressure sensor, could be set up as a Zeuch chamber to calculate the mass flow rate using Equation 24.

# 5 Setup functionality verification and first measurements

To test the general performance of the developed experimental setup, a number of exploratory experiments have been conducted to test the functioning of the setup and identify initial trends in performance behaviour. Note that, due to a breakdown of the selected 100DX pump and subsequent repair lead times, the decision was made to adopt a Teledyne ISCO 500D high-pressure pump into the setup. The relatively low maximum pressure of this pump equates to approximately 340 bar, and the syringe volume is 0.5 L.

The measurements that are presented in this chapter are all conducted with a baseline set of injection parameters, presented in Table 3. Unless stated otherwise, the recorded force signals are all obtained from a single nozzle orifice on the 7-hole CRIP2 injector. The rail pressure is capped by the maximum syringe pressure, whilst the fuel temperature is consistently only 2 °C higher than the ambient temperature of the laboratory (18 °C). Since marginal injection-to-injection differences might exist, the average force signal over a number of 25 injections is calculated (see section 5.2) to nullify the random error that stems from the injection-to-injection differences. The injection frequency is limited by the speed of the pressure feedback control of the syringe pump and the size of the fuel rail volume. For the 500D pump, the rail volume is approximately five times higher than that of the 100DX pump. Additionally, it is hypothesised that the pressure controller of the 500D pump is quicker than the 100DX controller. A frequency of 2 Hz proved adequate in managing a constant rail pressure at the start of solenoid energising (SOE). A higher injection frequency shortens the duration of the experiment, but can alter the injection parameters if the rail pressure requirement at SOE is not met. An example of an experiment where the injection frequency is too high is shown in Figure 5.1, where the legend denotes the injection number in a set of 100 injections. From the figure, it is clear that the feedback controller cannot ensure a consistent rail pressure at SOE. Therefore, the average pressure over an injection initially drops during the first couple of injections, after which it reaches a—lower than targeted—equilibrium pressure state at SOE conditions. To limit the influence of triboelectric noise in the amplified signal, a low-pass filter with cut-off frequency of 5kHz is used on the charge amplifier.

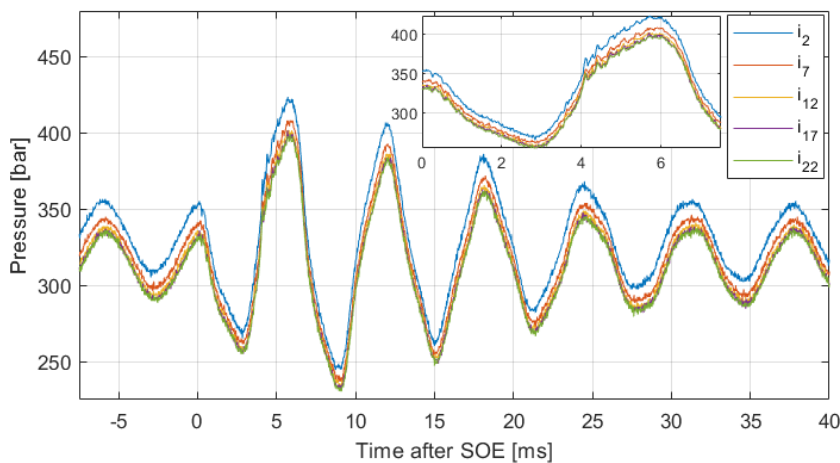


Figure 5.1: Effects of too high injection frequency on rail pressure. Targeted pressure of 340 bar, injection frequency of 20 Hz

Table 3: Baseline injection parameters

Parameter	Rail pressure	Fuel temperature	Sampling rate	No. of injections	Injection frequency	LP filter
Value	340 bar	20 °C	50000 Hz	25	2 Hz	5 kHz

## 5.1 Injector solenoid actuation

The characteristics of the injector driver output signal must be verified, such that the actuation of the injector is consistent for a wide variety of input settings. Also, the functioning of the injector driver can be validated, by comparing the input settings to the output parameters. Figure 5.2 shows an example of the injector driver TTL input voltage and measured driver output current profile, for a pre-injection with  $ET = 0.1$  ms, followed by a main injection with  $ET = 1$  ms and dwell time of 1 ms. Note that the output voltage of the injector driver was set at a constant 50 V. The shape of the current profile of the main injection can be explained by three parameters, the peak current, peak time, and hold current. After initiation by the TTL pulse, the injector driver outputs a high ( $\approx 16.8$  A) peak current for a sustained amount of time (the peak time), that quickly lifts the injector needle out of the needle seat. In order to avoid overheating and potential breakdown of the injector solenoid, the current is then lowered to the hold current (approximately 12 A) for the remainder of the injection energising duration. The total energising duration is controlled by the length of the TTL input pulse.

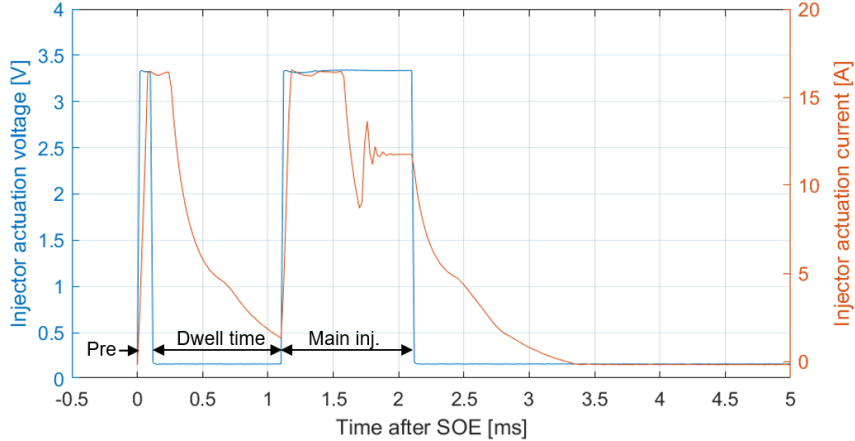


Figure 5.2: TTL actuation voltage and injector current

The current profile that is sent to the injector solenoid is not optimal. Firstly, the optimum current profile parameters are, unfortunately, not supplied by the manufacturer of the injector, Bosch. Accordingly, the parameters that are implemented were obtained from an available dataset of an older experimental setup that is no longer in use at the ZEL. The dataset contained only imprecise current profile information, and no information on the driver output voltage. A second factor is the sub-optimal performance of the injector driver. The driver allows a maximum peak current of 16.8 A, whilst the available dataset revealed a maximum value of approximately 17.5 A. Figure 5.2 further shows deficiencies in the beginning and ending phase of the current profile. After triggering, it takes approximately 0.08 ms before current peak conditions are reached, effectively introducing a slight temporal shift to the actuation. Additionally, there is a long “trailing” current slope visible after the TTL pulse stops. This trail elongates the effective ET of

both the pre- and main injection. This unwanted effect is especially visible in the current profile of the pre-injection, where even the peak current duration is already longer than the length of the TTL pulse.

For consistent measurements, it is important that the output of the injector driver exactly follows the input parameters as selected by the user of the setup. While the sub-optimal current injector driver output profile accommodates injections at 340 bar, this might not be the case at higher injection pressures. In fact, such behaviour was already observed in an initial exploratory experiment at higher injection pressure. In that particular experiment, a change in main injection energising time did not result in a longer injection duration, because the hold current setting was not correct.

## 5.2 Injection-to-injection variation

Consistent functioning of the setup throughout an experiment is necessary for obtaining correct, consistent measurement data. Possible inconsistent behaviour in consecutive injections can be caused by variations in injector actuation profiles, momentum sensor behaviour, or pressure oscillations that can affect injection dynamics. Figures 5.3 and 5.4 show the momentum flow rate and rail pressure fluctuation of the first five individual, non-averaged, injections in a set of 100 injections. The figures show that the injection-to-injection differences are minor, indicating that a relatively small set of 25 injections per experiment is adequate. The figures also show that the injection-to-injection differences are not a factor of the injection number. This observation, however, is only true provided that the pressure at the SOI remains stable throughout the experiment: during an experiment with a higher injection frequency, as seen in Figure 5.1, a drift in the injection pressure results in reduced repeatability of the momentum flow rate measurements.

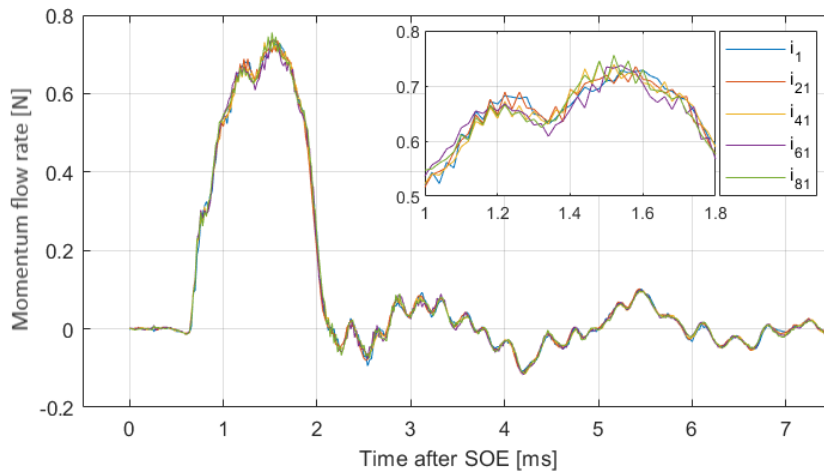


Figure 5.3: Momentum flow rate of 5 individual injections in a recording. All cases with ET of 1 ms, target diameter of 7.5 mm, and a target-to-nozzle distance of 7.5 mm

In Figure 5.3, the momentum step due to entrainment phenomena (see section 4.4.3), is visible in the initial rising slope of the measured force. Additionally, a non-random fluctuation in the quasi-static flow regime is observed. Note that the time after SOE at which the initial force increase is observed, is not purely representative of the injector hydraulic delay. This is due to a temporal shift, induced by the non-zero target-to-nozzle



distance. Note that this temporal shift will also affect the accuracy of the observed EOI, as the shift affects the entire measured trace. For future reference, the hydraulic delay for a certain set of injection parameters can be determined by placing the spray target directly at the nozzle exit, or approximated by comparing the start of the rising slope of the momentum flow rate signal of two identical injections at different target-to-nozzle distances. In the latter case, however, the non-constant velocity of the fuel spray due to the slowing down of the head of the spray cause by air entrainment, must be taken into consideration.

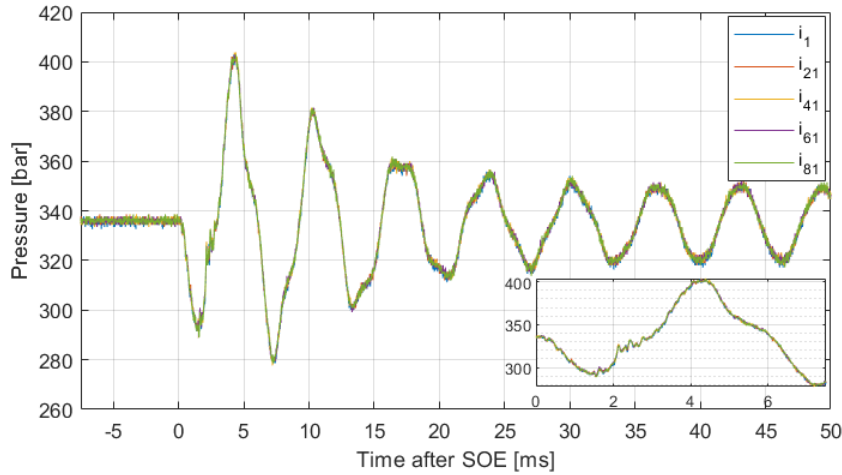


Figure 5.4: Rail pressure traces belonging to injections of Figure 5.3

In Figure 5.4, the fuel pressure in the common rail is shown during the injections shown in Figure 5.3. The figure shows large oscillations in the fuel rail due to the sudden release of pressure when the injector needle opens. At EOI, the pressure has dropped to approximately 290 bar, indicating a pressure fluctuation ratio of 15%. The fluctuation ratio is expected to increase with longer injection duration. For this particular ET, the pressure stabilises after approximately 100 ms. The minor differences in the pressure traces between individual injections demonstrates the major advantage in pressure control that the 500DX syringe pump holds over a conventional common rail pump such as is used with the EHPC.

### 5.3 Injector needle vibration

In all conducted measurements, it is observed that the measured force does not immediately decrease to zero after EOI. Instead, a vibration, which has a negligible injection-to-injection variation within a set of injections, appears in the signal. The magnitude and duration of this behaviour is not clearly observed in previous work in literature. The same can be said about the small force drop just before the “quasi” SOI, which is believed to originate from the same source as the vibration after EOI. It is believed that a vibration, generated by the injector needle actuation, is sensed and thus measured by the force sensor. Figure 5.5 shows the differences in measured momentum flow rate between “injection A” (identical to the injection set of Figure 5.3) and a reference experiment with  $ET = 1$  ms injections, but where the sensor is rotated away from the spray. In the reference experiment, similar vibrational behaviour is observed after SOE, and continues past EOI,

indicating that the vibration originates from the injector needle actuation. If the reference force trace is subtracted from “injection A”, the oscillation remains, albeit with smaller magnitude. Because, for the two cases, the sensor orientation about the rotation axis  $\theta$  is not identical, this might indicate that the characteristics of the measured vibration are a function of the sensor position in the injection chamber.

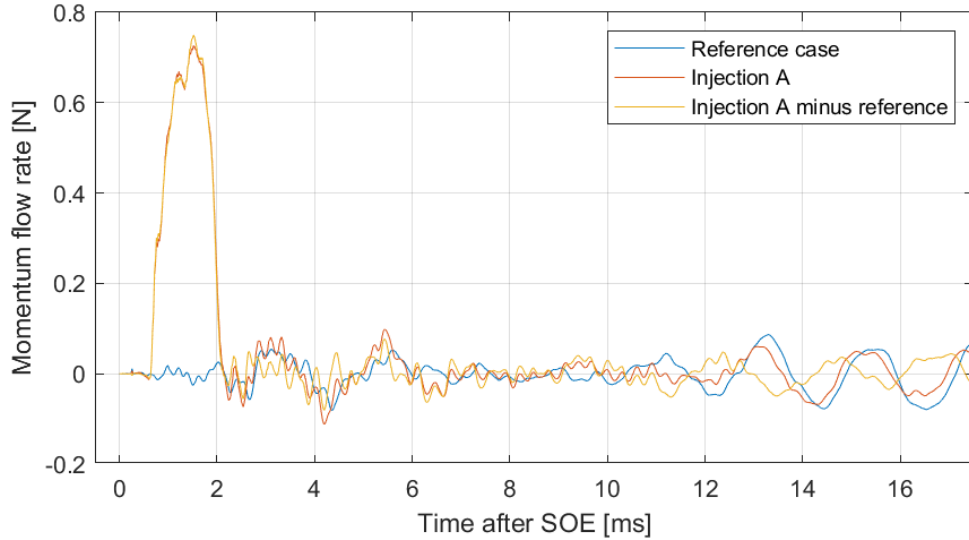


Figure 5.5: Suspected influence of needle actuation vibration on force measurement. All cases with ET of 1 ms, target diameter of 7.5 mm, and a target-to-nozzle distance of 7.5 mm

## 5.4 Sensor alignment sensitivity

Figure 5.6 illustrates how the measured momentum flow rate is affected by the level of alignment between the force sensor and nozzle hole. A misalignment is simulated by

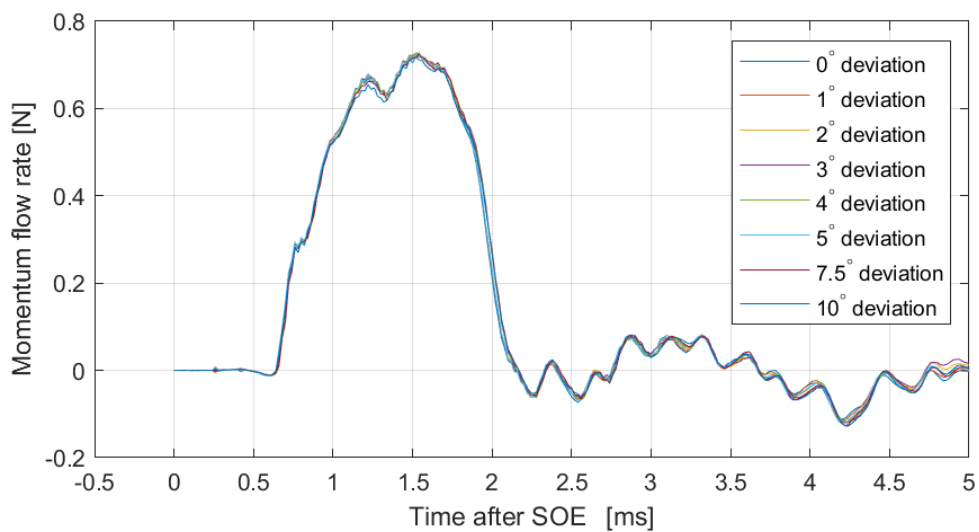


Figure 5.6: Influence of sensor misalignment on recorded momentum flow rate signal. All cases with ET of 1 ms, target diameter of 7.5 mm, and a target-to-nozzle distance of 7.5 mm

rotating the force sensor away from the nozzle hole in the  $\theta$  axis of Figure 4.5. Because both the  $\theta$  and  $\phi$  axis coincide at the nozzle, it is expected that a misalignment in any of the two axes results in the same result on the measured signal. The figure illustrates that even a substantial misalignment, much larger than the achievable resolution of the Thorlabs rotation stages, does not significantly influence the momentum flow rate measurement. Indeed, if the error due to misalignment at maximum measured momentum flow rate is calculated for the cases in Figure 5.6, it approximately scales to  $1 - \cos(\alpha)$ .

## 5.5 Target size and target-to-nozzle distance

Figures 5.7 and 5.8 show the influence of the spray target diameter and target-to-nozzle distance on the measured momentum flow rate signal. Although Figure 5.7 seems to suggest that the target diameter has a negligible influence on the measured momentum flow rate, Figure 5.8 proves that target with too large diameter can be influenced by neighbouring sprays when the distance to the injector becomes too small ( $L=2.5$  mm). In this case, the target is hit by two additional sprays, both at an angle of  $51.4^\circ$  to the main spray. The additional contribution of these sprays amounts to a maximum of 0.78 N. If the correlation for error due to misalignment (subsection 5.4) is used, the approximation is equal to 0.89 N. Furthermore, a smaller, lighter target ought to decrease the signal error due to the acceleration sensitivity of the sensor. Figure 5.8 especially shows the

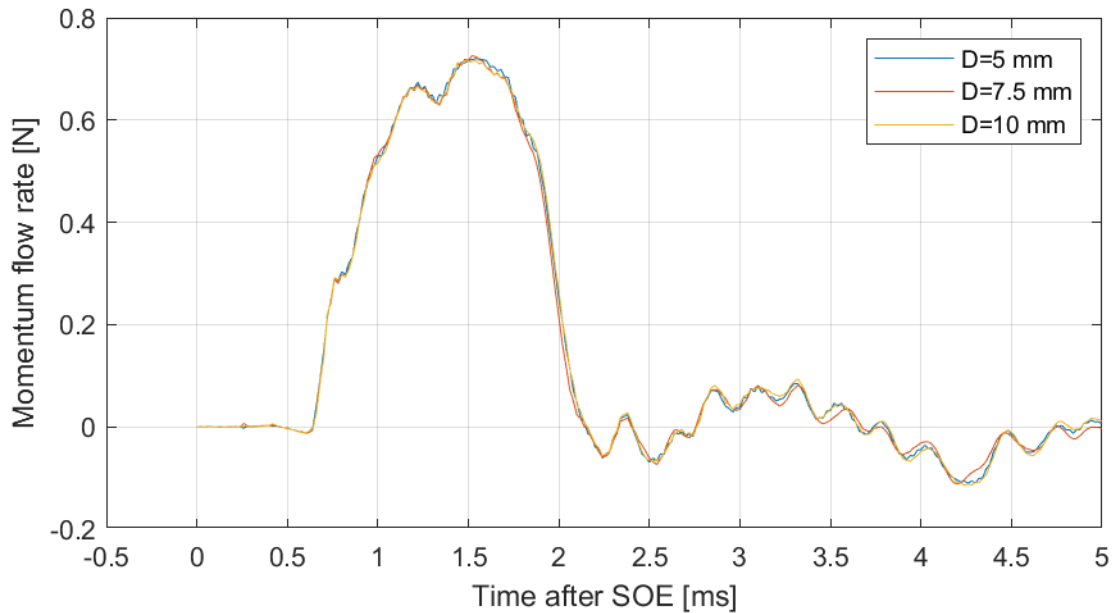


Figure 5.7: Influence of spray target diameter ( $D$ ) on measured momentum flow rate. All cases with 1 ms ET, and 7.5 mm target-to-nozzle distance

advantages of a small target-to-nozzle distance. Both the temporal error in the injector hydraulic delay, and the magnitude of the momentum step in the rising edge decrease in size when the target-to-nozzle distance decreases. The two figures show that, ideally, the target-to-nozzle distance is as small as possible with a target diameter that is just large enough to capture a single spray in its entirety.

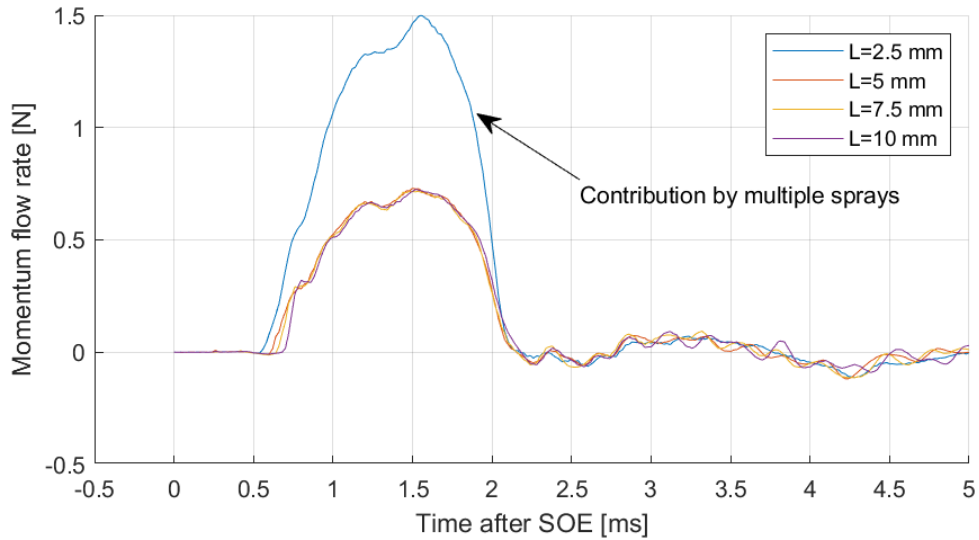


Figure 5.8: Influence of target-to-nozzle distance ( $L$ ) on measured momentum flow rate. All cases with 1 ms ET, and 10 mm target diameter

## 5.6 Hole-to-hole variation

In Figure 5.9, it is shown that the current experimental setup has the possibility to demonstrate differences in momentum flow behaviour between individual holes of an injector. The figure shows the injection-averaged measured force for three individual holes, evenly spaced on the same injector tip, where “hole 1” denotes the same hole that is used in all other measurements in section 5. The magnitude in the quasi-steady portion differs slightly amongst holes 1 and 2, and hole 3, whilst there are also clear differences visible amongst the holes when investigating the observed hydraulic delay. Since the target-to-nozzle distance is the same for all cases in the figure, this shows a direct correlation to the physical hydraulic delay. With the use of the proposed approach to obtain the mass flow rate from the momentum flow rate, these hole-to-hole differences can also be observed in the mass flow rate profiles.

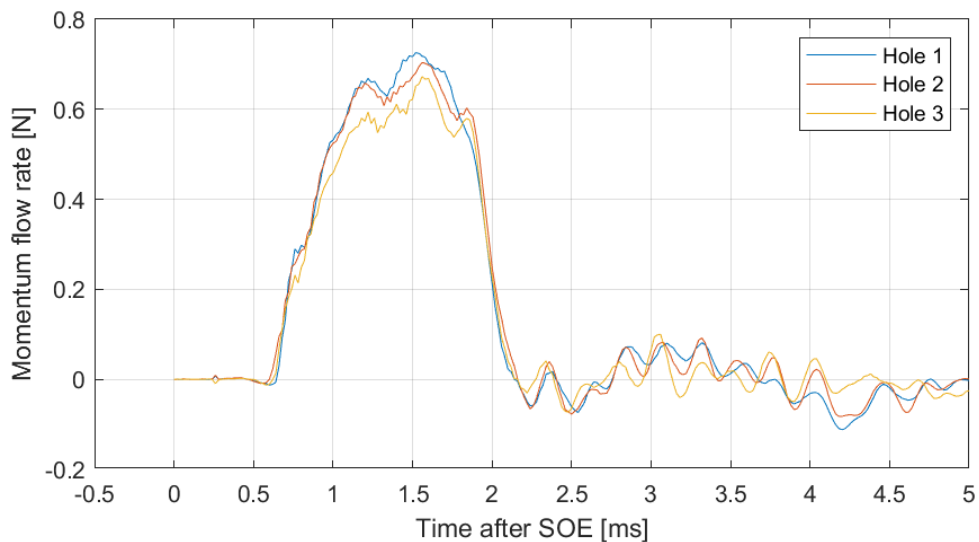


Figure 5.9: Variation in momentum flow rate between holes in the fuel injector. All cases with ET of 1 ms, target diameter of 7.5 mm, and a target-to-nozzle distance of 7.5 mm

An interesting observation is the substantial hole-to-hole variation in the magnitude of the oscillations observed after EOI. This could verify the hypothesis that the characteristics of the measured vibration depend on the orientation in space of the force sensor, given that the holes are evenly spaced with  $51.4^\circ$  increments in the  $\theta$  rotation axis of the sensor.

## 6 Conclusions

The current research project has succeeded in creating an experimental laboratory setup for the characterisation of liquid fuel injectors. A literature study was performed to find relevant information on the characterisation process and to determine the most suitable measurement technique to be implemented into the design of the physical setup. The necessary components for the setup were identified and described in detail, incorporating all relevant design features and decisions. After the components were manufactured and assembled to form a fully functioning prototype, a number of experiments were run to explore initial trends in the performance of the setup.

In the literature study of section 2, the relevant equations surrounding the characterisation of liquid nozzle flow have been presented. The equations that describe the gaseous characterisation coefficients at choked flow conditions were found through modification—following previous work in literature—of the characterisation equations for liquid flow. From the literature study, different measurement methods have been identified, such as the Bosch, Zeuch and jet impingement method. The methods have been assessed based on several criteria, such as quality of measurement, ease of implementation, measuring flexibility, and capabilities of doing measurements on individual nozzle orifices. Of the selected methods, the jet impingement force measuring technique was deemed the most suitable. Unlike the Bosch and Zeuch rate of injection methods, the jet impingement force method allows direct measuring of the transient momentum flow rate. The injection chamber requires only a single transducer for measuring the characterisation parameters, and the method allows for measurements on individual nozzle orifices of a multi-hole injector. With the jet impingement force method, the transient mass flow rate of individual nozzle orifices can be determined from the measured momentum flow rate via an approach as described by Naber and Siebers and Payri et al. [41, 31].

Due to time constraints, no specific experiments were conducted regarding weighing of the total injected fuel. Furthermore, an initial study on the influence of the target diameter and target-to-nozzle distance on the measured momentum flow rate has shown that a small target-to-nozzle distance can greatly reduce the magnitude of the momentum step in the initial rise of the injection signal. An initial study on the target diameter at a distance of 7.5 mm from the nozzle showed little influence of the target diameter on the measured momentum flow rate. When varying the distance between the nozzle and the target, more profound effects were found. With a shorter distance, an earlier rise in the momentum flow signal is detected. In the limit of decreasing this distance, however, the contribution of multiple sprays becomes apparent, disturbing the desired measurement. This highlights that a minimum target diameter that captures the full spray is preferred to facilitate the shortest distance to the nozzle orifice.

Instead of a common rail pump, a syringe pump was incorporated into the setup design. A syringe pump can deliver a more stable fuel pressure, and has a higher compatibility with exotic research fuels. Section 5.2 demonstrates that, with an appropriate injection frequency, both the rail pressure at SOE as well as the rail pressure throughout the injection show no clear variation between individual injections, therefore verifying the choice for a syringe pump. The injection chamber houses both the injector and the momentum sensor. The current chamber cannot be pressurised, but is able to house a wide variety of injector designs using dedicated adaptors.

The developed data acquisition system allows the user of the setup to send precisely timed actuation signals to the fuel injector. A multitude of settings can be customised in



the comprehensive front panel. It must be noted that the used injector driver showed signs of performance characteristics that are insufficient. Examples include the relatively low maximum peak current, and slow response time after the TTL actuation signal stopped.

## 7 Recommendations for future work

Whilst initially focusing on both liquid and gaseous fuels, the physical setup is currently optimised for liquid fuels such as diesel due to constraints in available time. However, the (possible) future addition of the possibility to test gaseous fuels—specifically gaseous hydrogen—has been incorporated in the design phase of the setup. For example, the selected measurement method is believed to be compatible with gaseous hydrogen, and the selected materials inside the injection chamber are able to withstand prolonged contact with gaseous hydrogen. It is believed that, with minimal effort, the current setup can be modified to house gaseous fuel injectors and accept gaseous injections. Only then can the applicability of the current measurement concept to the characterisation of gaseous injections be typified.

Two observations regarding the determination of the mass flow rate were made during the momentum flow rate experiments, however. Firstly, it was noticed that reaching an equilibrium state in the return flow tubing is difficult. Essentially, the capillary action of the diesel in the narrow Teflon tube induced a non-constant return flow rate. If this is the case, “zeroing” of the syringe pump cylinder does not yield a consistent amount of fuel in the fuel system. Secondly, after refilling the high-pressure fuel system with a different fuel, fully filling the return flow tube can require a considerable amount of time. This is necessary, since already present air bubbles in the tube further amplify the non-constant flow behaviour. Thus, the time required for the tube to fully fill and reach an equilibrium state severely limits the conversion speed of the setup for different fuels.

Due to long lead times and even unavailability of necessary components, the current high-pressure fuel system is rated for a maximum pressure of 700 bar, instead of an anticipated 2000 bar. Due to a breakdown of the originally incorporated 100DX syringe pump, a 500D syringe pump with an even lower pressure rating was installed in the setup. Nevertheless, the advantages of the syringe pump over a common rail pump have been demonstrated. At the time of writing, the control quality and speed of the internal feedback controller is unknown. Therefore, it is not well understood how the pressure controller affects the rail pressure during and after the injection. Hence, it is advised to further investigate this for future validation of the syringe pump in the setup. Regarding the sensor, a Kistler 9215A piezoelectric (non-IEPE) force sensor was selected to measure the momentum flow rate. Whilst a 9215A sensor was not available for purchase during the project, Kistler agreed to provide a comparable (albeit with lesser specifications) 9217A demonstration sensor for the duration of the project. The advice to purchase a 9215A still stands, especially for as long as the current injection chamber design remains unchanged.

In the measured momentum flow rate signals, a vibrational disturbance was identified that has a substantial detrimental effect on the quality of the obtained signal. The vibration presumably originates from the actuation of the injector solenoid and subsequent movement of the injector needle, and whilst displaying relatively little injection-to-injection variation, it undoubtedly has varying characteristics depending on the positioning of the force sensor. The factors contributing to the magnitude of the vibration must be identified. Although the injector needle is believed to be the main contributor, the sensor might also play a role in this, as well as the mechanical design of both the injection chamber and alignment fixture. The behaviour of the vibration as a function of the position of the sensor in space must also be further understood, in order to determine whether this indeed affects the vibration.

Apart from the points already discussed in this section, a number of practical inconveniences were identified during the initial experiments on the setup. Currently, the high impedance cable that connects the force sensor to the charge amplifier, travels through a hole in the lid on top of the sleeve away from the injection chamber. This means that, every time when the positioning of the sensor is adjusted, the cable must be uncoupled from the sensor. Uncoupling the cable in an environment where almost all components are covered in diesel fuel, can quickly result in contamination of the force sensor. Therefore, extreme care must be taken to prevent this from happening.

A second point of improvement is the shape of the base plate. Combined with the position of the O-ring that seals off the base plate and PMMA sleeve contact surface, it can cause fuel to accumulate right above the O-ring. This means that, when the PMMA sleeve is retracted from the base plate, the fuel spills past the O-ring. This phenomenon can be prevented by changing the geometry of the slope of the fuel collection face in the base plate, such that fuel can no longer accumulate above the O-ring.

# References

- [1] UNFCCC. The Paris Agreement, 2015.
- [2] Kistler Group. Sensors for Small Forces, 2016.
- [3] John B Heywood. *Internal Combustion Engine Fundamentals*. McGraw-Hill College, 1988.
- [4] Hannu Jääskeläinen and Magdi K. Khair. Diesel Fuel Injection, 2013.
- [5] Taku Tsujimura, Shohei Mikami, Norihisa Achiha, Yoshiroh Tokunaga, Jiro Senda, and Hajime Fujimoto. A study of direct injection diesel engine fueled with hydrogen. In *SAE Technical Papers*, 2003.
- [6] Glenn R. Bower and David E. Foster. A comparison of the bosch and zuech rate of injection meters. *SAE Technical Papers*, 1991.
- [7] R. Payri, J. M. García, F. J. Salvador, and J. Gimeno. Using spray momentum flux measurements to understand the influence of diesel nozzle geometry on spray characteristics. *Fuel*, 84(5):551–561, 3 2005.
- [8] Jaime Gimeno García. *Desarrollo y aplicación de la medida del flujo de cantidad de movimiento de un chorro diesel*. PhD thesis, Universidad Politécnica de Valencia, 2008.
- [9] EPA. Carbon Pollution from Transportation, 2017.
- [10] Bernd Heid, Christopher Martens, and Anna Orthofer. How hydrogen combustion engines can contribute to zero emissions, 2021.
- [11] Pavlos G. Aleiferis and Martino F. Rosati. Controlled autoignition of hydrogen in a direct-injection optical engine. *Combustion and Flame*, 159(7):2500–2515, 7 2012.
- [12] Ho Lung Yip, Aleš Srna, Anthony Chun Yin Yuen, Sanghoon Kook, Robert A. Taylor, Guan Heng Yeoh, Paul R. Medwell, and Qing Nian Chan. A Review of Hydrogen Direct Injection for Internal Combustion Engines: Towards Carbon-Free Combustion. *Applied Sciences 2019, Vol. 9, Page 4842*, 9(22), 11 2019.
- [13] Ali Mohammadi, Masahiro Shioji, Yasuyuki Nakai, Wataru Ishikura, and Eizo Tabo. Performance and combustion characteristics of a direct injection SI hydrogen engine. *International Journal of Hydrogen Energy*, 32(2):296–304, 2 2007.
- [14] Yasuo Takagi, Masakuni Oikawa, Ryota Sato, Yoshihisa Kojiya, and Yuji Mihara. Near-zero emissions with high thermal efficiency realized by optimizing jet plume location relative to combustion chamber wall, jet geometry and injection timing in a direct-injection hydrogen engine. *International Journal of Hydrogen Energy*, 44(18):9456–9465, 4 2019.
- [15] Thomas Wallner, Riccardo Scarcelli, Abhijeet M. Nande, and Jeffrey Naber. Assessment of Multiple Injection Strategies in a Direct-Injection Hydrogen Research Engine. *SAE International Journal of Engines*, 2(1):1701–1709, 6 2009.

- [16] W. Addy Majewsky and Hannu Jääskeläinen. Engine emission control, 2021.
- [17] Hannu Jääskeläinen. Fuel Injection for Clean Diesel Engines, 2017.
- [18] Hannu Jääskeläinen and Magdi K Khair. Common Rail Fuel Injection, 2010.
- [19] Kimitaka Yamane, Masakuni Oikawa, Tomonori Kitaura, Kouta Mawatari, Takashi Kondo, Yasuo Takagi, Yoshio Sato, and Yuichi Goto. A development of a high pressure H<sub>2</sub> gas injector with high response by using common-rail injection system for direct injection H<sub>2</sub> fuelled engines. In *16th World Hydrogen Energy Conference 2006, WHEC 2006*, volume 2, pages 1559–1565, 2006.
- [20] Chengjun Du, Sven Andersson, and Mats Andersson. The effect of cavitation on the estimation of fuel injection rates based on momentum flux measurements. *Fuel*, 238:354–362, 2 2019.
- [21] Philip G. Hill and Patric Ouellette. Transient turbulent gaseous fuel jets for diesel engines. *Journal of Fluids Engineering, Transactions of the ASME*, 121(1):93–101, 1999.
- [22] Alireza Hajialimohammadi, Daniel Edgington-Mitchell, Damon Honnery, Nader Montazerin, Amir Abdullah, and Mostafa Agha Mirsalim. Ultra high speed investigation of gaseous jet injected by a single-hole injector and proposing of an analytical method for pressure loss prediction during transient injection. *Fuel*, 184:100–109, 11 2016.
- [23] A. D. Birch, D. R. Brown, M. G. Dodson, and F. Swaffield. The structure and concentration decay of high pressure jets of natural gas. *Combustion Science and Technology*, 36(5-6):249–261, 1984.
- [24] B.C.R. Ewan and K. Moodie. Structure and velocity measurements in underexpanded jets. *Combustion Science and Technology*, Vol.45:275–288, 1986.
- [25] Qiang Cheng, Hulkkonen Tuomo, Ossi Tapani Kaario, and Larmi Martti. Spray dynamics of HVO and EN590 diesel fuels. *Fuel*, 245:198–211, 6 2019.
- [26] Jingyu Zhu, Olawole Abiola Kutu, and Keiya Nishida. An investigation of the effects of fuel injection pressure, ambient gas density and nozzle hole diameter on surrounding gas flow of a single diesel spray by the laser-induced fluorescence-particle image velocimetry technique. *International Journal of Engine Research*, 14(6):630–645, 12 2013.
- [27] R. Payri, B. Tormos, F. J. Salvador, and L. Araneo. Spray droplet velocity characterization for convergent nozzles with three different diameters. *Fuel*, 87(15-16):3176–3182, 11 2008.
- [28] Lucio Postrioti, Francesco Mariani, Michele Battistoni, and Alessandro Mariani. Experimental and numerical evaluation of diesel spray momentum flux. *SAE International Journal of Engines*, 2(2):287–299, 2010.
- [29] Wilhelm Bosch. The Fuel Rate Indicator: A New Measuring Instrument For Display of the Characteristics of Individual Injection. *SAE Technical Papers*, 2 1966.

- [30] Milan Marcic. Sensor for injection rate measurements. *Sensors*, 6(10):1367–1382, 2006.
- [31] R. Payri, G. Bracho, J. A. Soriano, P. Fernández-Yáñez, and O. Armas. Nozzle rate of injection estimation from hole to hole momentum flux data with different fossil and renewable fuels. *Fuel*, 279(November), 2020.
- [32] Andrea Cavicchi, Lucio Postrioti, Fabio Berni, Stefano Fontanesi, and Rita Di Gioia. Evaluation of hole-specific injection rate based on momentum flux measurement in GDI systems. *Fuel*, 263:116657, 3 2020.
- [33] Alessandro Mariani, Andrea Cavicchi, Lucio Postrioti, and Carmine Ungaro. A Methodology for the Estimation of Hole-to-Hole Injected Mass Based on Spray Momentum Flux Measurement. In *SAE Technical Papers*, number March. SAE International, 2017.
- [34] Benjamin W. Knox, Michael J. Franze, and Caroline L. Genzale. Diesel Spray Rate-of-Momentum Measurement Uncertainties and Diagnostic Considerations. *Journal of Engineering for Gas Turbines and Power*, 138(3):1–9, 2016.
- [35] Fueltech Solutions. CRU - Combustion Research Unit System Overview. Technical report, Fueltech Solutions, 2014.
- [36] Lucio Postrioti, Francesco Mariani, and Michele Battistoni. Experimental and numerical momentum flux evaluation of high pressure Diesel spray. *Fuel*, 98:149–163, 2012.
- [37] Rolf H Kuratle and André Signer. The Basic of Piezoelectric Measurement Technology. *Kistler Group*, 1999.
- [38] Lyle M Pickett, Julien Manin, Raul Payri, Michele Bardi, and Jaime Gimeno. Transient Rate of Injection Effects on Spray Development. *SAE International Journal of Engines*, pages 15–16, 2013.
- [39] Mikael Lindström and Hans Erik Ångström. Development of a fuel spray impulse measurement device and correlation with time resolved mass flow. *SAE Technical Papers*, 4970, 2009.
- [40] Hiro Hiroyasu and Masataka Arai. Structures of fuel sprays in diesel engines. In *SAE Technical Papers*. SAE International, 1990.
- [41] Jeffrey D Naber and Dennis L Siebers. Effects of Gas Density and Vaporization on Penetration and Dispersion of Diesel Sprays. *SAE Technical Papers*, (412), 1996.
- [42] Raúl Payri, Jaime Gimeno, Pedro Martí-Aldaraví, and Alberto Viera. Measurements of the mass allocation for multiple injection strategies using the rate of injection and momentum flux signals. *International Journal of Engine Research*, 22(4):1180–1195, 4 2021.
- [43] Bernhard Bill. Basic Theory of The Hammer Test Method. *Kistler Group*.



# Appendix A Pressure sensor calibration

To find the corresponding force of a pressure acting on the diaphragm of the pressure sensor, a correlation factor must be found. Whilst in theory the correlation factor can be calculated with  $F = p \cdot A$ , one cannot assume that the actual diaphragm area is equal to the effective pressure sensing surface area. Factors include the apparent surface area of the diaphragm touching the sensor housing, and the mechanical behaviour of the diaphragm sealing weld.

A better alternative is to perform a calibration procedure, based on actual measurements and can be done either statically or dynamically. For the static procedure calibrated weights are either placed on or removed from the top of the pressure transducer, in vertical orientation and with the charge amplifier time constant set to DC-mode to minimise signal drift. The measured static pressure can then be compared to the force of the weight acting on the the pressure diaphragm, in order to obtain the correlation factor. This must be done for multiple weights such that any non-linear behaviour may be identified. Whilst Figure A.1 does not show pressure traces of a pressure transducer calibration procedure, it shows the dynamic behaviour of a similar calibration procedure carried out with the Kistler 9217A force transducer. Case 1 and 2 are cases where the transducer is zeroed first and then the weight is put on top, whilst case 3 shows an example of the weight being removed from the transducer face. The difference in measurement stability and repeatability between the first two cases and case 3 is striking: it is well-nigh impossible to manually place the weight on the transducer face without any added kinetic or potential energy.

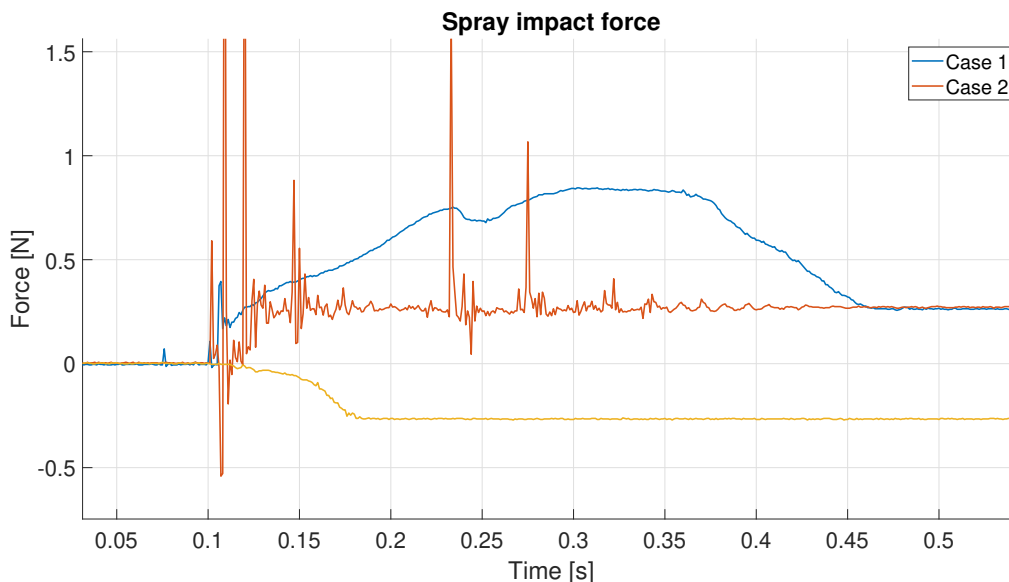


Figure A.1: Replication of a static force calibration for piezoelectric sensors.

In case 1, the weight is forcefully placed on top of the transducer, hence the prolonged magnitude in measured force. In case 2 the weight is “dropped” onto the transducer, inducing an initial peak force and vibration, caused by the weight bouncing on top of the sensing face. If instead, as in case 3, the weight is swiftly lifted off the pressure sensing face, the signal is much less perturbed and the repeatability of the calibration

procedure is improved. Drift, whilst not always clearly noticeable in the measurement, can be compensated for by determining the slope of the signal drift and extrapolating to the moment of placement or retraction of the calibrated weight. If the method of case 3 is followed, it is in addition much easier to compensate for the drift since both the drift can be estimated more accurately as well as the exact point of moving the weight can be determined much easier.

One of the downsides to statically calibrating a pressure sensor to force is that signal drift must be compensated for. A second possible limitation is that the transducer behaviour in the frequency domain cannot be evaluated. In an alternative dynamic calibration procedure as described by Bill [43], the pressure transducer is hit with an impulse force hammer. The force hammer is equipped with a piezoelectric force sensor on the tip and built-in accelerometer to analyse frequency response. Following Newton's third law, both sensors will experience the identical force and thus the peak pressure to force ratio can be determined. This is done for varying varying excitation frequencies to determine a correlation factor as a function of excitation frequency.

The dynamic calibration method is suggested for future use, as this allows expressing the correlation factor as a function of a dynamic parameter. In addition, it omits any potential introduction of signal perturbations such as drift. It requires purchasing a potentially expensive impulse force hammer, however, which must be kept in mind.